

1 **Optimizing sampling strategies in high-resolution paleoclimate records**

2

3 Niels J. de Winter<sup>1,2</sup> \*, Tobias Agterhuis<sup>1</sup>, Martin Ziegler<sup>1</sup>

4

5 <sup>1</sup>Department of Earth Sciences, Utrecht University, Princetonlaan 8a, 3584 CB Utrecht, the Netherlands

6 <sup>2</sup>AMGC research group, Vrije Universiteit Brussel, Pleinlaan 2, 1050 Brussels, Belgium

7

8 Correspondence to: Niels J. de Winter (n.j.dewinter@uu.nl)

9

10 **Abstract**

11 The aim of paleoclimate studies ~~to resolve~~ing climate variability from noisy proxy records can in essence  
12 be reduced to a statistical problem. The challenge is to extract meaningful information about climate  
13 variability from these records by reducing measurement uncertainty through ~~a combination of~~combining  
14 measurements of for proxies data while retaining the temporal resolution needed to assess the timing and  
15 duration of variations in climate parameters. In this study, we explore the limits of this compromise by testing  
16 different methods for combining proxy data (smoothing, binning and sample size optimization) on a  
17 particularly challenging paleoclimate problem: resolving seasonal variability in stable isotope records. We  
18 test and evaluate the effects of changes in the seasonal temperature and the hydrological cycle as well as  
19 changes in accretion rate of the archive and parameters such as sampling resolution and age model  
20 uncertainty on the reliability of seasonality reconstructions based on clumped and oxygen isotope analyses  
21 in 33 real and virtual datasets. Our results show that strategic combinations of clumped isotope analyses  
22 can significantly improve the accuracy of seasonality reconstructions compared to conventional stable  
23 oxygen isotope analyses, especially in settings where the isotopic composition of the water is poorly  
24 constrained. Smoothing data using a moving average often leads to an apparent dampening of the seasonal  
25 cycle, significantly reducing the accuracy of reconstructions. A statistical sample size optimization protocol  
26 yields more precise results than smoothing. However, the most accurate results are obtained through  
27 monthly binning of proxy data, especially in cases where growth rate or water composition cycles obscure  
28 the seasonal temperature cycle. Our analysis of a wide range of natural situations reveals that the effect of  
29 temperature seasonality on oxygen isotope records almost invariably exceeds that of changes in water  
30 composition. Thus, in most cases, oxygen isotope records allow reliable identification of growth seasonality  
31 as a basis for age modelling in the absence of independent chronological markers in the record. These  
32 specific findings allow us to formulate general recommendations for sampling and combining data in  
33 paleoclimate research and have implications beyond the reconstruction of seasonality. We briefly discuss  
34 the implications of our results for solving common problems in paleoclimatology and stratigraphy.

35

36 **1. Introduction**

37 Improving the resolution of climate reconstructions is a key objective in paleoclimate studies because it  
38 allows climate variability to be studied on different timescales and sheds light on the continuum of climate  
39 variability (Huybers and Curry, 2006). However, the temporal resolution of climate records is limited by the  
40 accretion rate (growth or sedimentation rate) of the archive and the spatial resolution of sampling for climate  
41 reconstructions, which is a function of the sample size required for a given climate proxy. This tradeoff  
42 between sample size and sampling resolution is especially prevalent when using state-of-the-art climate  
43 proxies which require large sample sizes, such as the carbonate clumped isotope paleothermometer ( $\Delta_{47}$ ;  
44 see applications in Rodríguez-Sanz et al., 2017; Briard et al., 2020; Caldarescu et al., 2021) or stable  
45 isotope ratios in specific compounds or of rare isotopes (e.g. phosphate-oxygen isotopes in tooth apatite,  
46 triple oxygen isotopes in speleothems or carbon isotopes of CO<sub>2</sub> in ice cores; Jones et al., 1999; Schmitt  
47 et al., 2012; Sha et al., 2020). The challenge of sampling resolution persists on a wide range of timescales:  
48 from attempts to resolve geologically short-lived (kyr-scale) climate events from deep sea cores with low  
49 sedimentation rates (e.g. Stap et al., 2010; Rodríguez-Sanz et al., 2017) to efforts to characterize tidal or  
50 daily variability in accretionary carbonate archives (e.g. Warter and Müller, 2017; de Winter et al., 2020a).  
51 What constitutes "high-resolution" is therefore largely dependent on the specifics of the climate archive.

52 Sample size limitations are especially important in paleoseasonality reconstructions. Reliable archives for  
53 seasonality (e.g. corals, mollusks and speleothem records) are in high demand in the paleoclimate  
54 community, because the seasonal cycle is one of the most important cycles in Earth's climate and  
55 seasonality reconstructions complement more common long-term (kyr to -Myr) records of past climate  
56 variability (e.g. Morgan and van Ommen, 1997; Tudhope et al., 2001; Steuber et al., 2005; Steffensen et  
57 al., 2008; Denton et al., 2005; Huyghe et al., 2015; Vansteenberghe et al., 2019). A more detailed  
58 understanding of climate dynamics at the human timescale is increasingly relevant for improving climate  
59 projections (IPCC, 2013). Unfortunately, the growth and mineralization rates of archives that capture high-  
60 resolution variability (~~rarely only~~ exceeding 10 mm/yr in rare exceptions, e.g. Johnson et al., 2019) limit the  
61 number and size of samples that can be obtained at high temporal resolutions (e.g. Mosley-Thompson et  
62 al., 1993; Passey and Cerling, 2002; Treble et al., 2003; Goodwin et al., 2003). In addition, accurate dating

63 ~~of climate archives~~ positioning of samples within the seasonal cycle is challenging. In absence of fine-scale  
64 ~~growth markings (e.g. daily laminae in mollusk shells; e.g. Schöne et al., 2005; de Winter et al., 2020a),~~  
65 ~~this dating problem relies on modelling or interpolation of the growth of the archive, which introduces~~  
66 ~~uncertainty on the age of samples (e.g. Goodwin et al., 2009; Judd et al., 2018). These problems is-are~~  
67 exacerbated by the fact that accurate methods for climate reconstructions ~~often-may~~ require comparatively  
68 large sample sizes, ~~while methods relying on smaller sample sizes or~~ rely on uncertain assumptions. A case  
69 in point is the popular carbonate stable oxygen isotope temperature proxy ( $\delta^{18}\text{O}_c$ ) which relies on  
70 assumptions of the water composition ( $\delta^{18}\text{O}_w$ ) that become progressively more uncertain further back in  
71 geological history (e.g. Veizer and Prokoph, 2015). ~~Contrarily~~In contrast, the clumped isotope proxy ( $\Delta_{47}$ )  
72 does not rely on this assumption but requires larger amounts of sample (e.g. Müller et al., 2017)

73 A promising technique for circumventing sample size limitations is to analyze larger numbers of small  
74 aliquots from the same sample or from similar parts of the climate archive. These smaller aliquots typically  
75 have poor precision but averaging multiple aliquots into one estimate while propagating the measurement  
76 uncertainty leads to a more reliable estimate of the climate variable (Dattalo, 2008; Meckler et al., 2014;  
77 Müller et al., 2017; Fernandez et al., 2017). This approach yields improved sampling flexibility since aliquots  
78 can be combined in various ways after measurement. It also allows outlier detection at the level of individual  
79 aliquots, thereby spreading the risk of instrumental failure and providing improved control on changes in  
80 measurement conditions that may bias results.

81 Previous studies have applied several different methods for combining data from paleoclimate records to  
82 reduce analytical noise or higher order variability, and extract variability with a specific frequency (e.g. a  
83 specific orbital cycle or seasonality; e.g. Lisiecki and Raymo, 2005~~4~~; Cramer et al., 2009). These data  
84 reduction approaches can in general be categorized into **smoothing** techniques, in which a sliding window  
85 or range of neighboring datapoints is used to smooth high resolution records (see e.g. Cramer et al., 2009)  
86 or **binning** techniques, in which the record is divided into equal bins in the sampling direction (e.g. time,  
87 depth or length in growth direction; e.g. Lisiecki and Raymo, 2004; Rodríguez-Sanz et al., 2017). In addition,  
88 a third approach is proposed here based on **optimization** of sample size for dynamic binning of data along  
89 the climate cycle using a moving window in the domain of the climate variable (as opposed to the sampling

90 domain) combined with a T-test routine (see section 2.1). All three approaches have advantages and  
91 caveats.

92 In this study, we explore the (dis)advantages of these three data reduction approaches by testing their  
93 reliability in resolving seasonal variability in sea surface temperature (SST) and water stable oxygen isotope  
94 composition ( $\delta^{18}\text{O}_w$ ), both highly sought-after variables in paleoclimate research. We compare  
95 reconstructions of SST and  $\delta^{18}\text{O}_w$  in real and virtual datasets from accretionary carbonate archives (e.g.  
96 shells, corals and speleothems) using the clumped isotope thermometer ( $\Delta_{47}$ ) combined with stable oxygen  
97 isotope ratios of the carbonate ( $\delta^{18}\text{O}_c$ ).

98

## 99 2. Methods

### 100 2.1 Reconstruction approaches

101 Throughout the remainder of this work, the three approaches for combining data for reconstructions are  
102 defined as follows (see also Fig. 1):

103 **Smoothing** refers to the reconstruction of SST and  $\delta^{18}\text{O}_w$  based on **moving averages** of  $\Delta_{47}$  and  $\delta^{18}\text{O}_c$   
104 records (Fig. 1B). For every dataset, the full possible range of moving window sizes (from 1 sample to the  
105 full length of the record) for SST and  $\delta^{18}\text{O}_w$  reconstructions was explored. The window size that resulted in  
106 the most significant difference between maximum and minimum  $\Delta_{47}$  values (based on a student's T-test)  
107 was applied to reconstruct SST and  $\delta^{18}\text{O}_w$  from  $\Delta_{47}$  and  $\delta^{18}\text{O}_c$  records. SST and  $\delta^{18}\text{O}_w$  were calculated for  
108 all case studies using a combination of empirical temperature relationships by Kim and O'Neil (1997;  $\delta^{18}\text{O}_c$ -  
109  $\delta^{18}\text{O}_w$ -temperature relationship) and Bernasconi et al. (2018;  $\Delta_{47}$ -temperature relationship). To obtain  $\delta^{18}\text{O}_w$   
110 values, the  $\delta^{18}\text{O}_c$ -  $\delta^{18}\text{O}_w$ -temperature relationship (Kim and O'Neil, 1997) was solved for  $\delta^{18}\text{O}_w$  using the  
111 temperature reconstruction obtained from  $\Delta_{47}$  measurements. Here and in other approaches, a typical  
112 analytical uncertainty on measurements of  $\Delta_{47}$  (one standard deviation of 0.04‰) and  $\delta^{18}\text{O}_c$  (one standard  
113 deviation of 0.05‰) was used to include uncertainty due to measurement precision. These analytical  
114 uncertainties were chosen based on typical uncertainties reported for these measurements in the literature  
115 (e.g. Schöne et al., 2005; Huyghe et al., 2015; Vansteenberghe et al., 2016) and long-term precision

116 uncertainties obtained by measuring in-house standards using the MAT253+ with Kiel IV setup in the  
117 clumped isotope laboratory at Utrecht University (e.g. Kocken et al., 2019). The measurement uncertainty  
118 was propagated through all calculations using a Monte Carlo simulation ( $N = 1000$ ) in which  $\Delta_{47}$  and  $\delta^{18}\text{O}_c$   
119 records were randomly sampled from a normal distribution with the virtual  $\Delta_{47}$  and  $\delta^{18}\text{O}_c$  values as means  
120 and analytical uncertainties as standard deviations. [Resulting SST and  \$\delta^{18}\text{O}\_w\$  values were grouped into](#)  
121 [monthly time bins using the age model of the archive.](#)

122 **Binning** refers to reconstructions of SST and  $\delta^{18}\text{O}_w$  based on binning of  $\Delta_{47}$  and  $\delta^{18}\text{O}_c$  records into monthly  
123 time bins (**Fig. 1C**). The  $\Delta_{47}$  and  $\delta^{18}\text{O}_c$  data from each case study were grouped into monthly time bins and  
124 converted to SST and  $\delta^{18}\text{O}_w$  using the Kim and O'Neil (1997) and Bernasconi et al. (2018) formulae. Here  
125 too, Monte Carlo simulation ( $N = 1000$ ) was applied to propagate measurement uncertainties onto monthly  
126 SST and  $\delta^{18}\text{O}_w$  reconstructions. Note that the prerequisite for this method is that the data is aligned using  
127 a (floating) age model accurate enough to allow samples to be placed in the right bin. The age of virtual  
128 samples in this study is known so this prerequisite poses no problems in this case. However, in the fossil  
129 record this alignment might be less certain in [the](#) absence of accurate chronologies within the archive (e.g.  
130 through daily growth increments in mollusk shells; e.g. Schöne et al., 2008; Huyghe et al., 2019; see 4.1.3).

131 **Optimization** refers to reconstructions of SST and  $\delta^{18}\text{O}_w$  based on sample size optimization in  $\Delta_{47}$  records  
132 (**Fig. 1D**). In this approach aliquots of each [virtual](#)-dataset are ordered from warm (low  $\delta^{18}\text{O}_c$ ) to cold (high  
133  $\delta^{18}\text{O}_c$  data) samples, regardless of their position relative to the seasonal cycle. From this ordered dataset,  
134 increasingly large samples of multiple aliquots (from 2 aliquots to half the length of the record) are taken  
135 from both the warm ("summer") and the cold ("winter") side of the distribution. Summer and winter samples  
136 were kept equal (symmetrical grouping) to reduce the number of possible sample size combinations and  
137 allow for more efficient computation. However, asymmetrical grouping with differing sample sizes on the  
138 summer and winter ends of the  $\delta^{18}\text{O}_c$ -spectrum are possible (see 4.1.3 and 4.2.2). Sample sizes with  
139 significant difference in  $\Delta_{47}$  value between summer and winter groups ( $p \leq 0.05$  based on a student's T-  
140 test) were selected as optimal sample sizes. The moving window T-test in the proxy domain ensures that  
141 an optimal compromise is reached between high precision and resolving differences between seasonal  
142 extremes. For each successful sample size, SST and  $\delta^{18}\text{O}_w$  values were calculated from  $\Delta_{47}$  and  $\delta^{18}\text{O}_c$  data

143 according to Kim and O'Neil (1997) and Bernasconi et al. (2018) formulae. The relationship between SST  
144 and  $\delta^{18}\text{O}_w$  obtained from these reconstructions was used to convert all  $\Delta_{47}$  and  $\delta^{18}\text{O}_c$  data to SST and  
145  $\delta^{18}\text{O}_w$ , which are then grouped into monthly SST and  $\delta^{18}\text{O}_w$  reconstructions [along the archive's age model](#).  
146 Measurement uncertainties were propagated through the entire approach by Monte Carlo simulation (N =  
147 1000).

148 For comparison, we also include reconstructions based solely on  $\delta^{18}\text{O}_c$  measurements with an (often  
149 inaccurate) assumption of a constant  $\delta^{18}\text{O}_w$  (equal to the modern ocean value of 0‰ VSMOW), which form  
150 the most common method for carbonate-based temperature reconstructions in paleoclimate research (see  
151 e.g. Schöne et al., 2005; Westerhold et al., 2020; **Fig. 1A**; hereafter:  **$\delta^{18}\text{O}$** ). For these reconstructions,  $\delta^{18}\text{O}_c$   
152 records were grouped into monthly time bins with analytical uncertainties propagated using the Monte Carlo  
153 approach (N = 1000) and were directly converted to SST using the Kim and O'Neil (1997) temperature  
154 relationship.

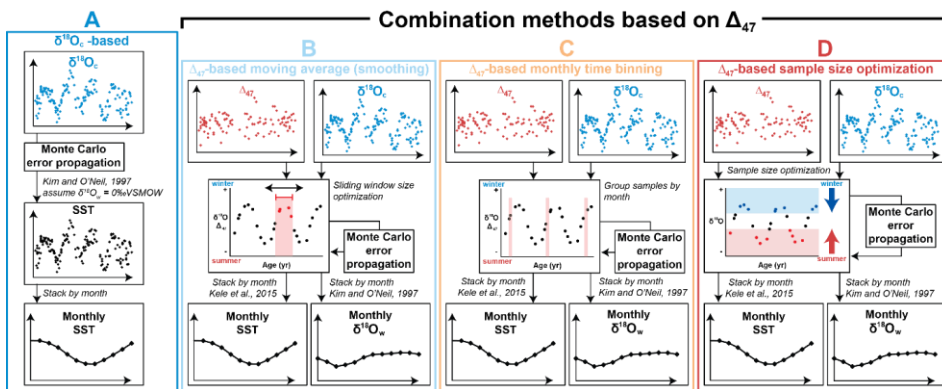
155 For each reconstruction, SST and  $\delta^{18}\text{O}_w$  results were aggregated into monthly averages, medians, standard  
156 deviations, and standard errors. Step by step documentation of calculations made for the three  $\Delta_{47}$ -based  
157 reconstruction approaches and the  $\delta^{18}\text{O}_c$  reconstructions are given in [Supplementary Data S7](#) and in the  
158 complementary R package (de Winter, 2021a).

## 159 **2.2 Benchmarks for accuracy and precision**

160 Accuracy and precision of reconstructions were evaluated against official USGS definitions of climate  
161 parameters (O'Donnell [et al. and Ignizio](#), 2012):

- 162 1. mean annual SST (MAT), defined as the average of all 12 monthly temperature reconstructions.
- 163 2. seasonal range in SST, defined as the temperature difference between warmest and coldest  
164 month.
- 165 3. mean annual  $\delta^{18}\text{O}_w$ , defined as the average of all 12 monthly  $\delta^{18}\text{O}_w$  reconstructions.
- 166 4. seasonal range in  $\delta^{18}\text{O}_w$ , defined as the  $\delta^{18}\text{O}_w$  difference between most enriched (highest  $\delta^{18}\text{O}_w$ )  
167 and most depleted (lowest  $\delta^{18}\text{O}_w$ ) monthly reconstruction.

168 Accuracy was defined as the absolute offset of the reconstructed climate parameter from the “true” value.  
 169 Precision was defined as the (relative) standard deviation of the reconstruction, as calculated from the  
 170 variability within monthly time bins resulting from Monte Carlo error propagation (see 2.1). An overview of  
 171 monthly SST and  $\delta^{18}\text{O}_w$  reconstructions using the four approaches in all cases is given in S4. Raw data  
 172 and figures of reconstructions of all cases using all sampling resolutions are compiled in S8.



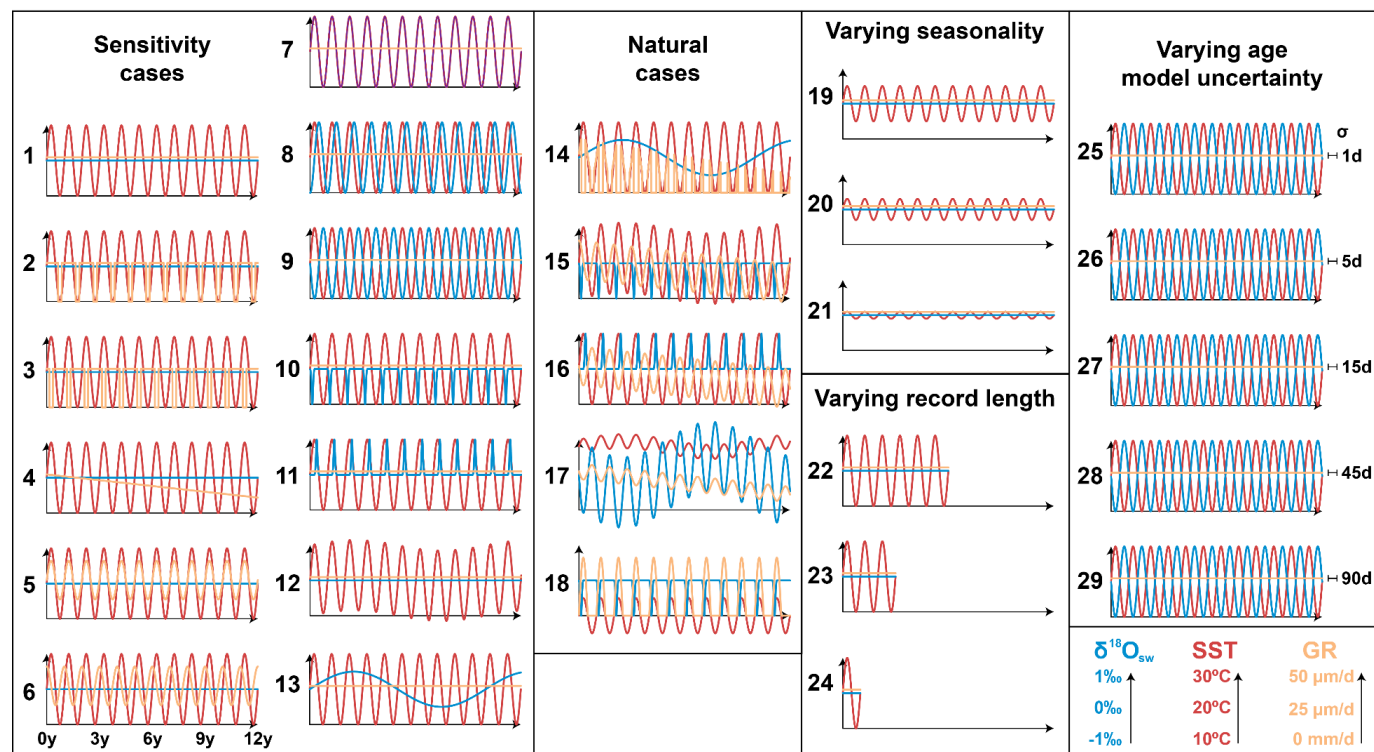
173  
 174 **Figure 1:** Schematic overview of the four approaches for seasonality reconstructions: (A)  $\delta^{18}\text{O}$ -based  
 175 reconstructions, assuming constant  $\delta^{18}\text{O}_w$ . (B) Reconstructions based on **smoothing**  $\delta^{18}\text{O}_c$  and  $\Delta_{47}$  data  
 176 using a moving average. (C) Reconstructions based on **binning**  $\delta^{18}\text{O}_c$  and  $\Delta_{47}$  data in monthly time bins.  
 177 (D) Reconstructions based on **optimization** of the sample size for combining  $\delta^{18}\text{O}_c$  and  $\Delta_{47}$  data (see  
 178 description in 2.1). Colored ~~curves-points~~ represent virtual  $\delta^{18}\text{O}_c$  (blue) and  $\Delta_{47}$  (red) series in sampling  
 179 domain. Black curves represent reconstructed monthly SST and  $\delta^{18}\text{O}_w$  averages.

### 180 181 2.3 SST and $\delta^{18}\text{O}_w$ datasets

182 The three reconstruction approaches were tested and compared based on three types of data: Firstly, a  
 183 set of datasets based on fully artificial environmental SST and  $\delta^{18}\text{O}_w$  data (case 1-29; see Fig. 2) converted  
 184 to virtual  $\Delta_{47}$  and  $\delta^{18}\text{O}_c$  records, data from a real specimen of a Pacific oyster (*Crassostrea gigas*, syn.  
 185 *Magallana gigas*) reported in Ullmann et al. (2010). Secondly, data based on actual measurements of  
 186 natural variability in SST and sea surface salinity (SSS; case 30-33) converted to virtual  $\Delta_{47}$  and  $\delta^{18}\text{O}_c$   
 187 records. Thirdly, measured proxy data from a real specimen of a Pacific oyster (*Crassostrea gigas*, syn.  
 188 *Magallana gigas*) compared to measured environmental (SST and  $\delta^{18}\text{O}_w$ ) data reported in Ullmann et al.  
 189 (2010). a set of datasets based on fully artificial SST and  $\delta^{18}\text{O}_w$  data (case 1-29; see Fig. 2) converted to  
 190 virtual  $\Delta_{47}$  and  $\delta^{18}\text{O}_c$  records.



## Virtual cases



191

192 **Figure 2:** Overview of time series of all virtual test cases. Colored curves represent time series of SST (red),  $\delta^{18}\text{O}_{\text{w}}$  (blue) and growth rate (orange,  
193 abbreviated as "GR"). Horizontal axes in all plots are 12 years long (see legend below case 6). Vertical axis of all plots has the same scale (SST:  
194 10 to 30°C;  $\delta^{18}\text{O}_{\text{w}}$ : -1 to +1‰; Growth rate: 0–50  $\mu\text{m}/\text{day}$ ; see legend in bottom right corner). Horizontal error bars and labels on the right side of  
195 cases 25-29 represent standard errors introduced on the age model (bars not to scale). The  $\delta^{18}\text{O}_{\text{c}}$  and  $\Delta_{47}$  records resulting from these virtual  
196 datasets are provided in **S6** (see also **Fig. 3** for natural examples).

Sensitivity cases		Natural cases	Varying seasonality	Varying age model uncertainty
1. Control	7. $\delta^{18}\text{O}_w$ seasonality in phase with SST	14. Full marine case with ontogenetic GR trend	19. Control case with reduced SST amplitude ( $\sim 5^\circ\text{C}$ )	25. Case 9 with $\pm 1$ day age model uncertainty
	8. $\delta^{18}\text{O}_w$ seasonality in antiphase with SST		20. Control case with reduced SST amplitude ( $\sim 3^\circ\text{C}$ )	
2. Growth stops $< 12^\circ\text{C}$	9. $\delta^{18}\text{O}_w$ seasonality lags SST by $\frac{1}{4}$ year	15. Coastal case with spring $\delta^{18}\text{O}_w$ decrease and decreasing GR trend	21. Control case with reduced SST amplitude ( $\sim 1^\circ\text{C}$ )	26. Case 9 with $\pm 5$ days age model uncertainty
3. Growth stops $> 28^\circ\text{C}$	10. Negative $\delta^{18}\text{O}_w$ in spring	16. Lagoonal case with summer $\delta^{18}\text{O}_w$ increase	Varying record length	27. Case 9 with $\pm 15$ days age model uncertainty
4. Linear decrease in GR	11. Positive $\delta^{18}\text{O}_w$ in summer	17. Tropical monsoon case with confined SST seasonality and strong multi-annual SST cycle		22. Control case shortened to 6 yr
5. GR seasonality in phase with SST	12. Multi-annual (5 yr) SST cycle	18. Worst-case scenario with growth limited to summer half of the year	23. Control case shortened to 3 yr	29. Case 9 with $\pm 90$ days age model uncertainty
6. GR seasonality lags SST by $\frac{1}{4}$ year	13. Multi-annual (5 yr) $\delta^{18}\text{O}_w$ cycle		24. Control case shortened to 1 yr	

197 **Table 1:** Overview of virtual cases 1-29 used to test the reconstruction methods. Case descriptions are  
198 abbreviated. Details on the SST, growth rate and  $\delta^{18}\text{O}_w$  included in each case are described in detail in **S1**.  
199 SST, growth rate and  $\delta^{18}\text{O}_w$  records of all cases are shown in **Fig. 2**. "GR" = growth rate.

200

201 2.3.1 Virtual cases **Cases 1-29: Virtual environmental data, virtual proxy data**

202 Virtual SST and  $\delta^{18}\text{O}_w$  time series were artificially constructed to test the effect of various SST and  $\delta^{18}\text{O}_w$   
203 scenarios on the effectivity of the reconstruction methods. The default test case (case 1) contained an ideal,  
204 12-year sinusoidal SST curve with a period of 1 year (seasonality), a mean value of  $20^\circ\text{C}$  and a seasonal  
205 amplitude of  $10^\circ\text{C}$ , a constant  $\delta^{18}\text{O}_w$  value of  $0\text{‰}$  and a constant growth rate of  $10\text{ mm/yr}$ . Other cases  
206 contain various deviations from this ideal case (see also **Fig. 2, Table 1** and **S1**):

- 207 • Linear and/or seasonal changes in growth rate, including growth stops (cases 2-6, 14-18)

- 208 • Seasonal and/or multi-annual changes in  $\delta^{18}\text{O}_w$  (cases 7-11, 13-18)
- 209 • Multi-annual trends in SST superimposed on the seasonality (cases 12, 15 and 17)
- 210 • Variations in the seasonal SST amplitude (cases 19-21)
- 211 • Change in the total length of the time series (cases 22-24)
- 212 • Variation in uncertainty on the age of each virtual datapoint (cases 25-29)

213 Comparison of the virtual time series (case 1-29; **Fig. 2**) with the natural variability (case 30-33; **Fig. 3**)  
214 shows that the virtual cases are not realistic approximations of natural variability in SST and  $\delta^{18}\text{O}_w$ . Natural  
215 SST and  $\delta^{18}\text{O}_w$  variability are not limited to the seasonal or multi-annual scale but contain a fair amount of  
216 higher order (daily to weekly scale) variability. To simulate this natural variability, we extracted the seasonal  
217 component of SST and  $\delta^{18}\text{O}_w$  variability from our highest resolution record of measured natural SST and  
218 SSS data (case 30: data from Texel, the Netherlands, see **2.3.2** and **Fig. 3**). The standard deviation of  
219 residual variability of this data after subtraction of the seasonal cycle was used to add random high-  
220 frequency noise to the SST and  $\delta^{18}\text{O}_w$  variability in virtual cases. Note that while sub-annual environmental  
221 variability can be approximated by Gaussian noise (Wilkinson and Ivany, 2002), this representation is an  
222 oversimplification of reality. In the case of our Texel data, the SST and SSS residuals are not normally  
223 distributed (Kolmogorov-Smirnov test:  $D = 0.010$ ;  $p = 7.2 \cdot 10^{-14}$  and  $D = 0.039$ ;  $p < 2.2 \cdot 10^{-16}$  for SST and  
224 SSS residuals respectively; see **S2-4**). SST and  $\delta^{18}\text{O}_w$  data from cases 1-29 was converted to the sampling  
225 domain and subsampled at a range of sampling resolutions following the same procedure applied to cases  
226 30-33 (see **2.3.2**).

227

228 *Modern oyster data*

229 Environmental SST and  $\delta^{18}\text{O}_w$  data from the Ligt Basin in Denmark (54°59.25N, 8°23.51E), where the  
230 modern oyster specimen lived, were obtained from local *in situ* measurements of SST and SSS described  
231 in Ullmann et al. (2010). Since direct, *in situ* measurements of  $\delta^{18}\text{O}_w$  variability at a high temporal resolution  
232 were not available,  $\delta^{18}\text{O}_w$  was estimated from more widely available SSS data using a mass balance  
233 (equation 1 and 2; following e.g. Ullmann et al., 2010).

234  $\delta^{18}O_{sw} = \delta^{18}O_{w,freshwater} * f + \delta^{18}O_{w,ocean} * (1 - f)$  (1)

235  $f = \frac{SSS_{sample} - SSS_{ocean}}{SSS_{freshwater} - SSS_{ocean}}$  (2)

236 ~~Here, we assume salinity ( $SSS_{sample}$ ) results from a mixture of a fraction ( $f$ ) isotopically light and low salinity~~  
237 ~~( $\delta^{18}O_{w,freshwater} = 8.5\text{‰}$ ;  $SSS_{freshwater} = 0$ ) freshwater and a fraction ( $1 - f$ ) ocean water ( $\delta^{18}O_{w,ocean} = 0\text{‰}$ ;~~  
238  ~~$SSS_{ocean} = 35$ ), with negative amounts of freshwater contribution ( $f < 0$ ) representing net evaporation~~  
239 ~~( $SSS_{sample} > SSS_{ocean}$ ). The value for  $\delta^{18}O_{w,freshwater}$  was based on the discharge weighted average  $\delta^{18}O_w$  of~~  
240 ~~water in the nearby Elbe and Weser rivers (see Ullmann et al., 2010). All  $\delta^{18}O_w$  values throughout the text~~  
241 ~~are with reference to the VSMOW scale. Contrary to the virtual datasets (cases 1-33; see 2.3.2 and 2.3.3),~~  
242 ~~the Ullmann et al. (2010) data was already available in the sampling domain, hence no subsampling was~~  
243 ~~required.~~

244 2.3.2 Cases 30-33: based on real climate data Measured environmental data, virtual proxy data

245 Four test cases were based on time series of real measured SST and SSS data from four different locations,  
246 selected to capture a variety of environments with different SST and SSS variability (see **Fig. 3**):

- 247 1. Tidal flats of the Wadden Sea near Texel, the Netherlands (case 30)
- 248 2. Great Barrier Reef in Australia (case 31)
- 249 3. Gulf of Aqaba between Egypt and Saudi Arabia (case 32)
- 250 4. Northern Atlantic Ocean east of Iceland (case 33).

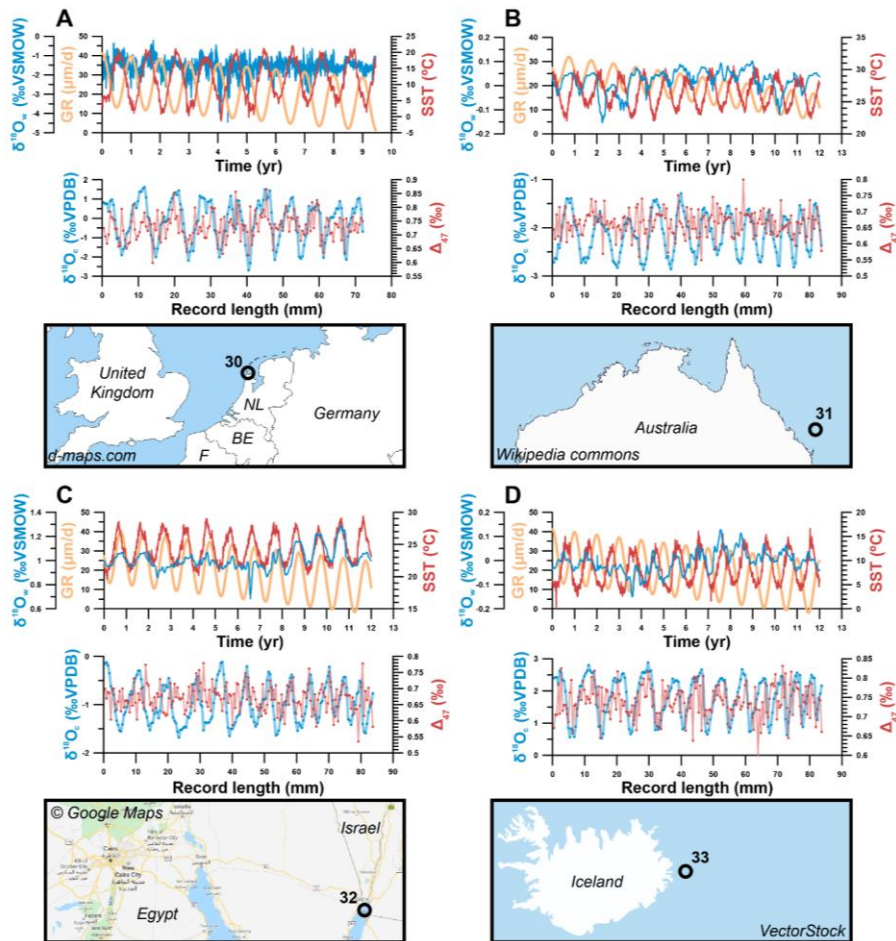
251 Daily measurements of SST and SSS for case 31-33 were obtained from worldwide open-access datasets  
252 of the National Oceanic and Atmospheric Administration (NOAA, 2020) and European Space Agency (ESA,  
253 2020) respectively. Hourly SST and SSS measured *in situ* in the Wadden Sea (case 30) were obtained  
254 from the Dutch Institute for Sea Research (NIOZ, Texel, the Netherlands). ~~Since direct, *in situ*~~  
255 ~~measurements of  $\delta^{18}O_w$  variability at a high temporal resolution are scarce,  $\delta^{18}O_w$  was estimated from (more~~  
256 ~~widely available) SSS data using the same mass balance described in 2.3.1. Since direct, *in situ*~~  
257 ~~measurements of  $\delta^{18}O_w$  variability at a high temporal resolution were not available,  $\delta^{18}O_w$  was estimated~~  
258 ~~from more widely available SSS data using a mass balance (equation 1 and 2; following e.g. Ullmann et~~  
259 ~~al., 2010):~~

260  $\delta^{18}O_{sw} = \delta^{18}O_{w,freshwater} * f + \delta^{18}O_{w,ocean} * (1 - f)$  (1)

261  $f = \frac{SSS_{sample} - SSS_{ocean}}{SSS_{freshwater} - SSS_{ocean}}$  (2)

262 Here, we assume salinity ( $SSS_{sample}$ ) results from a mixture of a fraction ( $f$ ) isotopically light and low-salinity  
263 ( $\delta^{18}O_{w,freshwater} = -8\text{‰}$ ;  $SSS_{freshwater} = 0$ ) freshwater and a fraction ( $1-f$ ) ocean water ( $\delta^{18}O_{w,ocean} = 0\text{‰}$ ;  
264  $SSS_{ocean} = 35$ ), with negative amounts of freshwater contribution ( $f < 0$ ) representing net evaporation  
265 ( $SSS_{sample} > SSS_{ocean}$ ). The value for  $\delta^{18}O_{w,freshwater}$  was based on the  $\delta^{18}O_w$  of rain in the Netherlands ( $-8\text{‰}$ ;  
266 Mook, 1970; Bowen, 2020). Applying this mass balance on the SSS record of the Wadden Sea tidal flats  
267 (case 30) results in  $\delta^{18}O_w$  values and a SSS- $\delta^{18}O_w$  relationship in agreement with measurements in this  
268 region (Harwood et al., 2008). SST and  $\delta^{18}O_w$  time series for all cases are given in [Supplementary Data](#)  
269 [S4](#) and natural cases are plotted in [Fig. 3](#).

270 For all virtual proxy datasets (cases 1-33), records of SST and  $\delta^{18}O_w$  were converted to the sampling  
271 domain (along the length of the record) by defining a virtual growth rate in the sampling direction. Adding  
272 this growth rate as a variable allowed us to test the sensitivity of approaches to changes in the extension  
273 rate of the archive, including hiatuses (growth rate = 0). This is important, because fluctuations in linear  
274 extension rate and periods in which no mineralization occurs (hiatuses or growth cessations) are common  
275 in all climate archives (e.g. Treble et al., 2003; Ivany, 2012). After conversion to the sampling domain, virtual  
276 aliquots were subsampled at equal distance from the SST and  $\delta^{18}O_w$  series of all cases using six sampling  
277 intervals: 0.1 mm, 0.2 mm, 0.45 mm, 0.75 mm, 1.55 mm and 3.25 mm. The four largest sampling intervals  
278 were chosen such that the standard growth rate (10 mm/yr) was not an integer multiple of the sampling  
279 interval (e.g. 0.45 mm instead of 0.5 mm, and 3.25 mm instead of 3 mm). This decision prevents sampling  
280 the same parts of the seasonal cycle (e.g. same months) every year, which biases both the mean value  
281 and the precision of monthly SST and  $\delta^{18}O_w$  reconstructions. This bias towards certain parts of the seasonal  
282 cycle is much stronger at low sample sizes (large sampling intervals) and is illustrated in the  
283 **Supplementary [Information Figure S2](#).**



284

285 **Figure 3:** Overview of the four cases of virtual data based on natural SST and SSS measurements explored  
 286 in this study. **(A)** Case 30: Tidal flats on the Wadden Sea, Texel, the Netherlands. **(B)** Case 31 Great Barrier  
 287 Reef, Australia). **(C)** Case 32: Gulf of Aqaba between Egypt and Saudi Arabia. **(D)** Case 33: Atlantic Ocean  
 288 east of Iceland. For all cases, graphs on top show environmental data, with SST plotted in red,  $\delta^{18}O_w$  in  
 289 blue and growth rate (abbreviated as "GR") in orange (as in **Fig. 2**). The graph below shows virtual  $\delta^{18}O_c$   
 290 (blue) and  $\Delta_{47}$  (red) records created from these data series using a sampling interval of 0.45 mm and  
 291 including analytical noise (see **3.3**). Note that the scale of vertical axes varies between plots.

292

293 2.3.3 Modern oyster data: *Measured environmental data, measured proxy data*

294 Environmental SST and  $\delta^{18}\text{O}_w$  data from the List Basin in Denmark (54°59.25N, 8°23.51E), where the  
 295 modern oyster specimen lived, were obtained from local *in situ* measurements of SST and SSS described  
 296 in Ullmann et al. (2010). Since direct, *in situ* measurements of  $\delta^{18}\text{O}_w$  variability at a high temporal resolution  
 297 were not available,  $\delta^{18}\text{O}_w$  was estimated from more widely available SSS data using a the mass balance  
 298 described in 2.3.2. (equation 1 and 2; following e.g. Ullmann et al., 2010):

299 
$$\delta^{18}\text{O}_{sw} = \delta^{18}\text{O}_{w,\text{freshwater}} * f + \delta^{18}\text{O}_{w,\text{ocean}} * (1 - f) \quad (1)$$

300 
$$f = \frac{\text{SSS}_{\text{sample}} - \text{SSS}_{\text{ocean}}}{\text{SSS}_{\text{freshwater}} - \text{SSS}_{\text{ocean}}} \quad (2)$$

301 Here, we assume salinity ( $\text{SSS}_{\text{sample}}$ ) results from a mixture of a fraction ( $f$ ) isotopically light and low salinity  
 302 ( $\delta^{18}\text{O}_{w,\text{freshwater}} = -8.5\text{‰}$ ;  $\text{SSS}_{\text{freshwater}} = 0$ ) freshwater and a fraction ( $1-f$ ) ocean water ( $\delta^{18}\text{O}_{w,\text{ocean}} = 0\text{‰}$ ;  
 303  $\text{SSS}_{\text{ocean}} = 35$ ), with negative amounts of freshwater contribution ( $f < 0$ ) representing net evaporation  
 304 ( $\text{SSS}_{\text{sample}} > \text{SSS}_{\text{ocean}}$ ). The value for  $\delta^{18}\text{O}_{w,\text{freshwater}}$  was based on the discharge weighted average  $\delta^{18}\text{O}_w$  of  
 305 water in the nearby Elbe and Weser rivers (see Ullmann et al., 2010). All  $\delta^{18}\text{O}_w$  values throughout the text  
 306 are with reference to the VSMOW scale. Contrary to the virtual datasets (cases 1-33; see 2.3.12 and  
 307 2.3.32), the Ullmann et al. (2010) data was already available in the sampling domain, hence no subsampling  
 308 was required.

309 *Virtual cases*

310 Virtual SST and  $\delta^{18}\text{O}_w$  time series were artificially constructed to test the effect of various SST and  $\delta^{18}\text{O}_w$   
 311 scenarios on the effectivity of the reconstruction methods. The default test case (case 1) contained an ideal,  
 312 42-year sinusoidal SST curve with a period of 1 year (seasonality), a mean value of 20°C and a seasonal  
 313 amplitude of 10°C, a constant  $\delta^{18}\text{O}_w$  value of 0‰ and a constant growth rate of 10 mm/yr. Other cases  
 314 contain various deviations from this ideal case (see also Fig. 2, Table 1 and S1):

- 315 ● Linear and/or seasonal changes in growth rate, including growth steps (cases 2-6, 14-18)
- 316 ● Seasonal and/or multi-annual changes in  $\delta^{18}\text{O}_w$  (cases 7-11, 13-18)
- 317 ● Multi-annual trends in SST superimposed on the seasonality (cases 12, 15 and 17)

Formatted: Normal, No bullets or numbering

318 ● Variations in the seasonal SST amplitude (cases 19-21)  
319 ● Change in the total length of the time series (cases 22-24).  
320 ● Variation in uncertainty on the age of each virtual datapoint (cases 25-29)

321 Comparison of the virtual time series (case 1-20; **Fig. 2**) with the natural variability (case 30-33; **Fig. 3**)  
322 shows that the virtual cases are not realistic approximations of natural variability in SST and  $\delta^{18}O_w$ . Natural  
323 SST and  $\delta^{18}O_w$  variability are not limited to the seasonal or multi-annual scale but contain a fair amount of  
324 higher order (daily to weekly scale) variability. To simulate this natural variability, we extracted the seasonal  
325 component of SST and  $\delta^{18}O_w$  variability from our highest resolution record of measured natural SST and  
326 SSS data (case 30: data from Texel, the Netherlands, see **2.3.2** and **Fig. 3**). The standard deviation of  
327 residual variability of this data after subtraction of the seasonal cycle was used to add random high-  
328 frequency noise to the SST and  $\delta^{18}O_w$  variability in virtual cases. Note that while sub-annual environmental  
329 variability can be approximated by Gaussian noise (Wilkinson and Ivany, 2002), this representation is an  
330 oversimplification of reality. In the case of our Texel data, the SST and SSS residuals are not normally  
331 distributed (Kolmogorov-Smirnov test:  $D = 0.010$ ;  $p = 7.2 \cdot 10^{-4}$  and  $D = 0.039$ ;  $p < 2.2 \cdot 10^{-16}$  for SST and  
332 SSS residuals respectively; see **S2-4**). SST and  $\delta^{18}O_w$  data from cases 1-29 was converted to the sampling  
333 domain and subsampled at a range of sampling resolutions following the same procedure applied to cases  
334 30-33 (see **2.3.2**).

335



336 **2.4 Conversion to  $\delta^{18}\text{O}_c$  and  $\Delta_{47}$  data**

337 After subsampling, SST and  $\delta^{18}\text{O}_w$  series (cases 1-33) were converted to  $\delta^{18}\text{O}_c$  and  $\Delta_{47}$  using a carbonate  
338 model based on empirical relationships between  $\Delta_{47}$  and  $\delta^{18}\text{O}_c$  with ~~and~~ SST and  $\delta^{18}\text{O}_w$  (equation 3 and 4;  
339 Kim and O'Neil, 1997; Kele et al., 2015; Bernasconi et al., 2018) and the conversion of  $\delta^{18}\text{O}$  values from  
340 VSMOW to VPDB scale (equation 5; Brand et al., 2014).

341 
$$\Delta_{47} = \frac{0.0449 \cdot 10^6}{(SST + 273.15)^2} + 0.167 \quad (3)$$

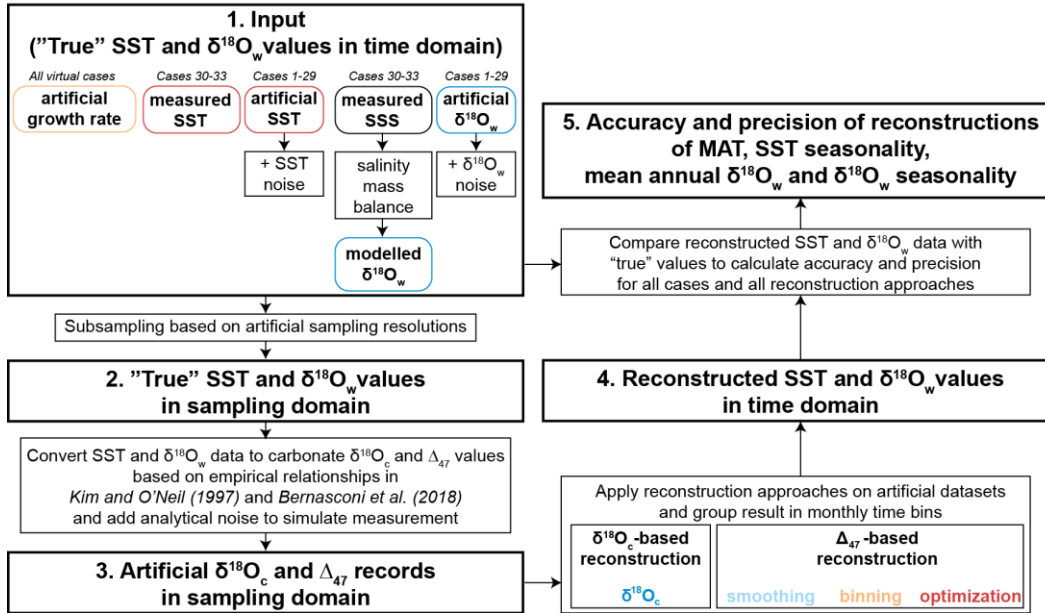
342 
$$1000 * \ln \left( \frac{\left( \frac{^{18}\text{O}}{^{16}\text{O}} \right)_{\text{CaCO}_3}}{\left( \frac{^{18}\text{O}}{^{16}\text{O}} \right)_{\text{H}_2\text{O}}} \right) = 18.03 * \left( \frac{10^3}{(SST + 273.15)} \right) - 32.42 \quad (4)$$

343 
$$\delta^{18}\text{O}_{\text{VPDB}} = 0.97002 * \delta^{18}\text{O}_{\text{VSMOW}} - 29.98 \quad (5)$$

344 For the ~~real-modern~~ oyster data (Ullmann et al., 2010; see **2.3.34**), only the  $\Delta_{47}$  data needed to be created  
345 because  $\delta^{18}\text{O}_c$  was directly measured. As a result, each case study yielded records of  $\Delta_{47}$  and  $\delta^{18}\text{O}_c$  in the  
346 sampling domain and corresponding “true” SST and  $\delta^{18}\text{O}_w$  records in the time domain, allowing assessment  
347 of the reliability of the reconstruction approaches in different scenarios- (~~Figure-Fig. 4~~). The result of  
348 applying these steps is illustrated on case 31 (Great Barrier reef data, **Fig. 5**). All calculations for creating  
349  $\Delta_{47}$  and  $\delta^{18}\text{O}_c$  series in sampling domain were carried out using the open-source computational software R  
350 (R core team, 2013), and scripts for these calculations are given in **Supplementary Data S7** and compiled  
351 in the documented R package “seasonalclumped” (de Winter, 2021a). All  $\Delta_{47}$  and  $\delta^{18}\text{O}_c$  datasets are  
352 provided in **Supplementary Data SS6**.

353

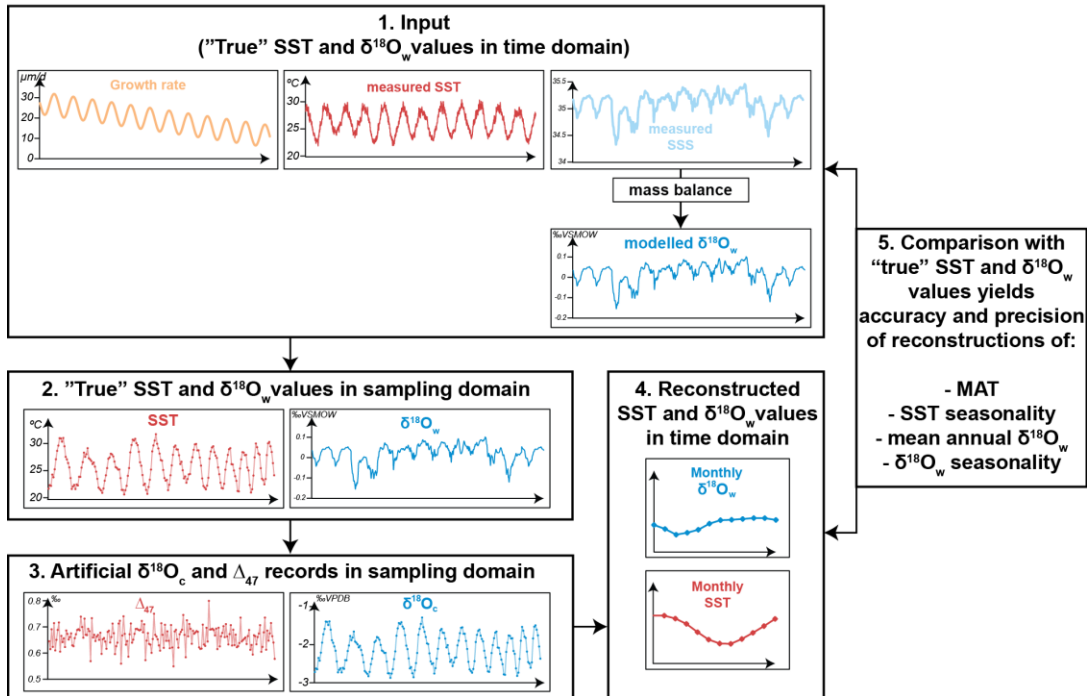
Workflow for creating virtual datasets and testing reconstruction approaches



354

355 **Figure 4:** Flow diagram showing the steps taken to create virtual data ( $\Delta_{47}$  and  $\delta^{18}\text{O}_c$ ; cases 1-33) and  
 356 compare results of SST and  $\delta^{18}\text{O}_w$  reconstructions with the actual SST and  $\delta^{18}\text{O}_w$  data the record was  
 357 based on (counterclockwise direction). Steps 1-3 outline the procedure for creating virtual  $\Delta_{47}$  and  $\delta^{18}\text{O}_c$   
 358 datasets (see sections 2.3 and 2.4), step 4 shows the application of the different reconstruction methods  
 359 on this virtual data (see Fig. 2 for details) and step 5 illustrates how the reconstructions are compared  
 360 with the original ("true") SST and  $\delta^{18}\text{O}_w$  data to calculate accuracy and precision of the reconstruction  
 361 approaches. Note that step 1 is different for cases 1-29 (based on fully artificial SST and  $\delta^{18}\text{O}_w$  records;  
 362 2.3.31) than for cases 30-33 (SST and  $\delta^{18}\text{O}_w$  records based on real SST and SSS data; see 2.3.2).

Workflow for creating virtual datasets and testing reconstruction approaches:  
 Example for case 31 (Great Barrier Reef satellite data)



363  
 364 **Figure 5:** An example of the steps highlighted in Fig. 4 using case 31 (Great Barrier Reef data) to illustrate  
 365 the data processing steps. Virtual data plots include normally distributed measurement uncertainty on  $\Delta_{47}$   
 366 and  $\delta^{18}\text{O}_c$ .

367

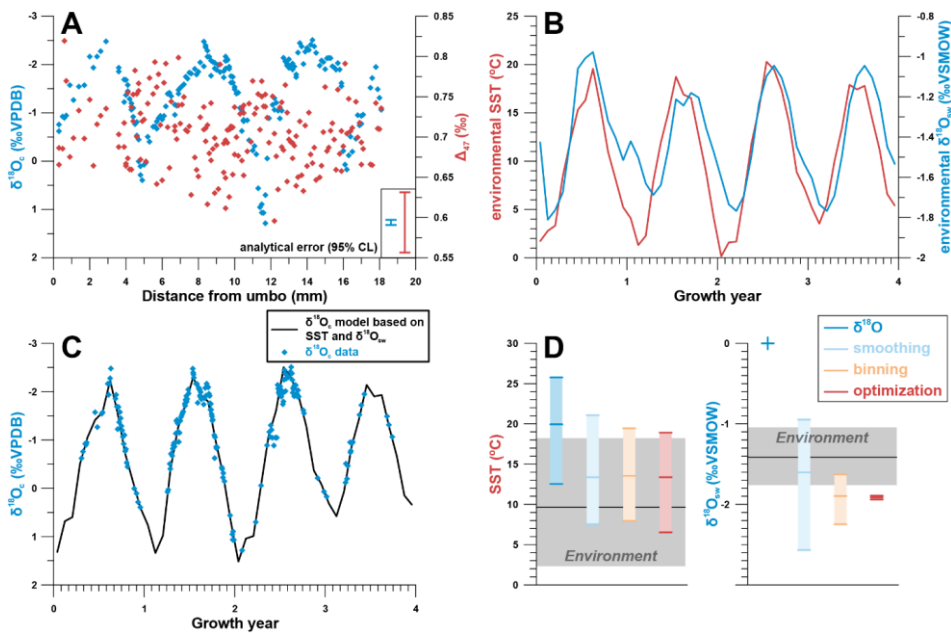
### 368 3. Results

#### 369 3.1 Real example

370 Measured ( $\delta^{18}\text{O}_c$ ) and simulated ( $\Delta_{47}$ ) data from the Pacific oyster from the Danish List Basin yielded  
371 estimates of SST and  $\delta^{18}\text{O}_w$  seasonality using all reconstruction approaches (Fig. 6). While a model of shell  
372  $\delta^{18}\text{O}_c$  based on SST and SSS data closely approximates the measured  $\delta^{18}\text{O}_c$  record (Fig. 6C), basing SST  
373 reconstructions solely on  $\delta^{18}\text{O}_c$  data without any *a priori* knowledge of  $\delta^{18}\text{O}_w$  variability (assuming constant  
374  $\delta^{18}\text{O}_w$  equal to the global marine value) leads to high inaccuracy in ~~SST seasonality and~~ mean annual SST  
375 (Fig. 6D). Note that, in absence of significant  $\delta^{18}\text{O}_w$  seasonality (as in this case study), seasonal  
376 temperature range reconstructions from  $\delta^{18}\text{O}_c$  measurements can be very accurate. However, assuming  
377 constant  $\delta^{18}\text{O}_w$  year-round may introduce considerable bias (see Fig. 7 and 8). The in-phase relationship  
378 between SST and SSS (Fig. 6B) slightly dampens the seasonal  $\delta^{18}\text{O}_c$  cycle, causing underestimation of  
379 temperature seasonality, while a negative mean annual  $\delta^{18}\text{O}_w$  value in the List Basin biases SST  
380 reconstructions towards higher temperatures. In terms of SST reconstructions, the **smoothing**, **binning**  
381 and **optimization** approaches based on  $\Delta_{47}$  and  $\delta^{18}\text{O}_c$  data yield more accurate reconstructions, albeit with  
382 a reduced seasonality and a bias towards the summer season. The latter is a result of severely reduced  
383 growth rates in the winter season, which was therefore undersampled (see Fig. 6A and 6C). Approaches  
384 including  $\Delta_{47}$  data also yield far more accurate  $\delta^{18}\text{O}_w$  estimates than the  **$\delta^{18}\text{O}$**  approach. However, the  
385 accuracy of  $\delta^{18}\text{O}_w$  seasonality and mean annual  $\delta^{18}\text{O}_w$  estimates is low in these approaches too, largely  
386 because of the limited sampling resolution, especially in winter. The **optimization** approach suffers from  
387 the strong in-phase relationship between SST and SSS, which obscures the difference between the  $\delta^{18}\text{O}_w$   
388 effect and the temperature effect on shell carbonate. Yet, disentangling SST from  $\delta^{18}\text{O}_w$  seasonality is  
389 central to the success of the approach (see 3.4). Fig. 6D does not show the ~~reproducibility-error~~precision  
390 on SST and  $\delta^{18}\text{O}_w$  estimates, which is much ~~larger~~lower for the **smoothing** approach than for the **binning**  
391 an **optimization** approaches due to the limited data in the winter seasons (see **Supplementary Data S56**).  
392 These results show that several properties of carbonate archives, such as growth rate variability, phase  
393 relationships between SST and  $\delta^{18}\text{O}_w$  seasonality and sampling resolution, can impact the reliability of

Formatted: Line spacing: Double

394 paleoseasonality reconstructions. The virtual and real data cases in this study were tailored to test the  
 395 effects of these archive properties more thoroughly.



396  
 397 **Figure 6:** (A) Plot of  $\delta^{18}O_c$  and (virtual)  $\Delta_{47}$  data from a modern Pacific oyster (*Crassostrea gigas*; see  
 398 Ullmann et al., 2010). (B) shows SST and  $\delta^{18}O_w$  data from the List Basin (Denmark) in which the oyster  
 399 grew. (C) shows the fit between  $\delta^{18}O_c$  data and modelled  $\delta^{18}O_c$  calculated from SST and  $\delta^{18}O_w$  on which  
 400 the shell age model was based. (D) Shows a summary of the results of different approaches for  
 401 reconstructing SST and  $\delta^{18}O_w$  from the  $\delta^{18}O_c$  and  $\Delta_{47}$  data. The vertical colored bars show the reconstructed  
 402 seasonal variability using all methods with ticks indicating warmest month, coldest month, and annual  
 403 mean. The grey horizontal bars show the actual seasonal variability in the environment. Precision ~~errors~~  
 404 standard deviation on monthly reconstructions are not shown but are given in S4.

405  
 406 **3.2 Case-specific results**

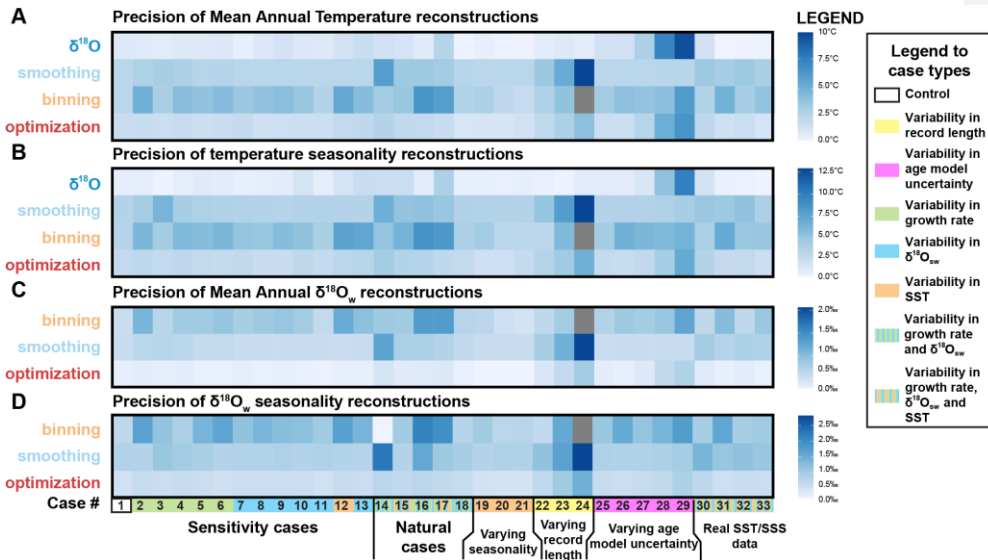
407 A case-by-case breakdown of the precision (Fig. 7) and accuracy (Fig. 8) of reconstructions using the four  
 408 approaches shows that reliability of reconstructions varies significantly between approaches and is highly  
 409 case-specific. In general, precision is highest in  $\delta^{18}O$  reconstructions, followed by **optimization** and  
 410 **binning**, with **smoothing** generally yielding the worst precision. Average ~~precision~~ standard deviations of  
 411 the underperforming methods (**binning** and **smoothing**) are up to 2-3 times larger than those of  $\delta^{18}O$  (e.g.

Formatted: Font: Not Bold

412 respectively 3.9°C and 3.5°C vs. 1.3°C for  $\delta^{18}\text{O}$  MAT reconstructions; see also **Supplementary**  
413 **Information**). It is worth noting that precision on  $\delta^{18}\text{O}$ -based estimates is mainly driven by measurement  
414 precision (which is better for  $\delta^{18}\text{O}_c$  than for  $\Delta_{47}$  measurements, see section 4.1.1).  $\Delta_{47}$ -based reconstructions  
415 lose precision due to the higher measurement error on  $\Delta_{47}$  measurements and the method used for  
416 combining measurements for seasonality reconstructions. On a case-by-case basis, the hierarchy of  
417 approaches can vary, especially if strong variability in growth rate is introduced, such as in case 14, where  
418 the size of hiatuses in the record increases progressively, or in case 18, in which half of the year is missing  
419 due to growth hiatuses (see **Table 1**, **Supplementary Data S1** and **S4**). Of the  $\Delta_{47}$ -based methods  
420 (**smoothing**, **binning** and **optimization**), **optimization** is rarely outcompeted in terms of precision in both  
421 SST and  $\delta^{18}\text{O}_w$  reconstructions.

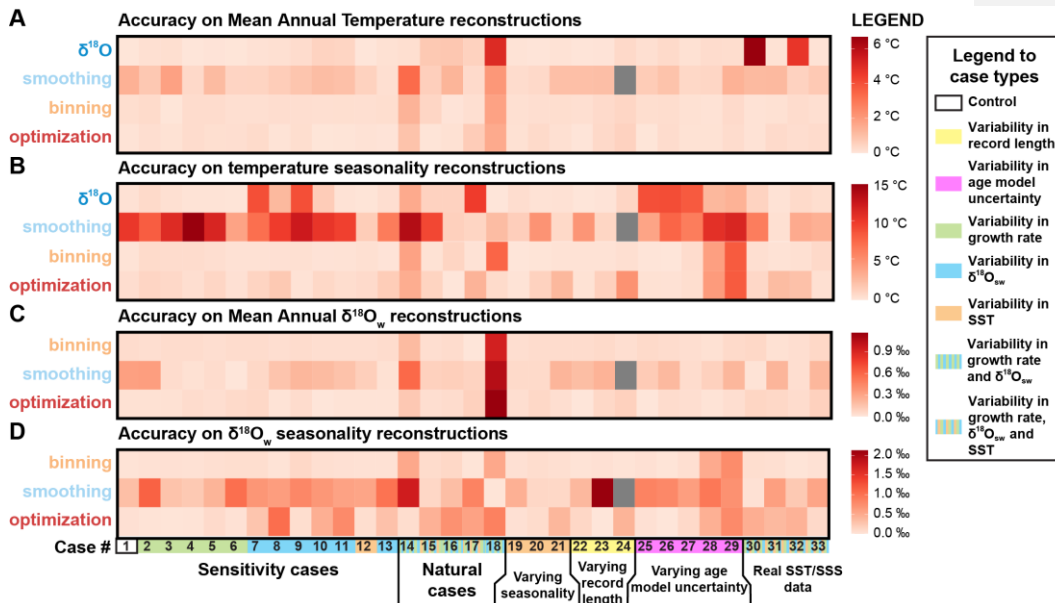
422 The comparison based on precision alone is misleading, as the most precise approach ( $\delta^{18}\text{O}$ ) runs the risk  
423 of being highly inaccurate (offsets exceeding 4°C on some MAT reconstructions; see **Fig. 7C8A**), especially  
424 in cases based on natural SST and SSS measurements (case 30-33). The **smoothing** approach also often  
425 yields highly inaccurate results, especially in cases with substantial variability in  $\delta^{18}\text{O}_w$  (e.g. case 9-11; **Fig.**  
426 **8**). Accuracy of **optimization** and **binning** outcompete the other methods in most circumstances. **Binning**  
427 outperforms **optimization** in reconstructions of  $\delta^{18}\text{O}_w$  seasonality, making it overall the most accurate  
428 approach. Interestingly, **optimization** is less accurate specifically in cases with sharp changes in growth  
429 rate in summer (e.g. cases 11, 14, 16 and 17), while **binning** performs better in these cases.  
430 Reconstructions of mean annual SST and  $\delta^{18}\text{O}_w$  in case 18 are especially inaccurate regardless of which  
431 method is applied. This extreme case with growth only during one half of the year combined with seasonal  
432 fluctuations in both SST and  $\delta^{18}\text{O}_w$  presents a worst-case scenario for seasonality reconstructions leading  
433 to strong biases in mean annual temperature reconstructions. In situations like case 18, the **optimization**  
434 approach is most accurate in MAT and SST seasonality reconstructions, but  $\delta^{18}\text{O}_w$  is more accurately  
435 reconstructed using the **binning** approach. Finally, it is worth noting that in natural situations (**Fig. 3**),  
436 variability in SST almost invariably has a larger influence on  $\delta^{18}\text{O}_c$  and  $\Delta_{47}$  records than  $\delta^{18}\text{O}_w$ , such that  
437 fluctuations in  $\delta^{18}\text{O}_c$  records closely follow the SST seasonality even in cases with relatively large  $\delta^{18}\text{O}_w$   
438 variability (e.g. case 30). Chronologies based on these  $\delta^{18}\text{O}_c$  fluctuations are therefore generally accurate.

Formatted: Font: Bold



440 **Figure 7:** Overview of precision (propagated standard deviation of variability within reconstructions, see  
 441 **2.2**) of reconstructions of mean annual temperature (**A**), seasonal temperature range (**B**), mean annual  
 442  $\delta^{18}O_w$  (**C**) and seasonal range in  $\delta^{18}O_w$  (**D**), with higher values (darker colors) indicating lower precision  
 443 (more variability between reconstructions) based on average sampling resolution (sampling interval of 0.45  
 444 mm). The different cases on the horizontal axis are color coded by their difference from the control case  
 445 (case 1; see legend on the right-hand side). Grey boxes indicate cases for which reconstructions were not  
 446 successful. All data on precision (standard deviation values) is provided in [Supplementary Data S4](#).

Formatted: Font: Italic



447

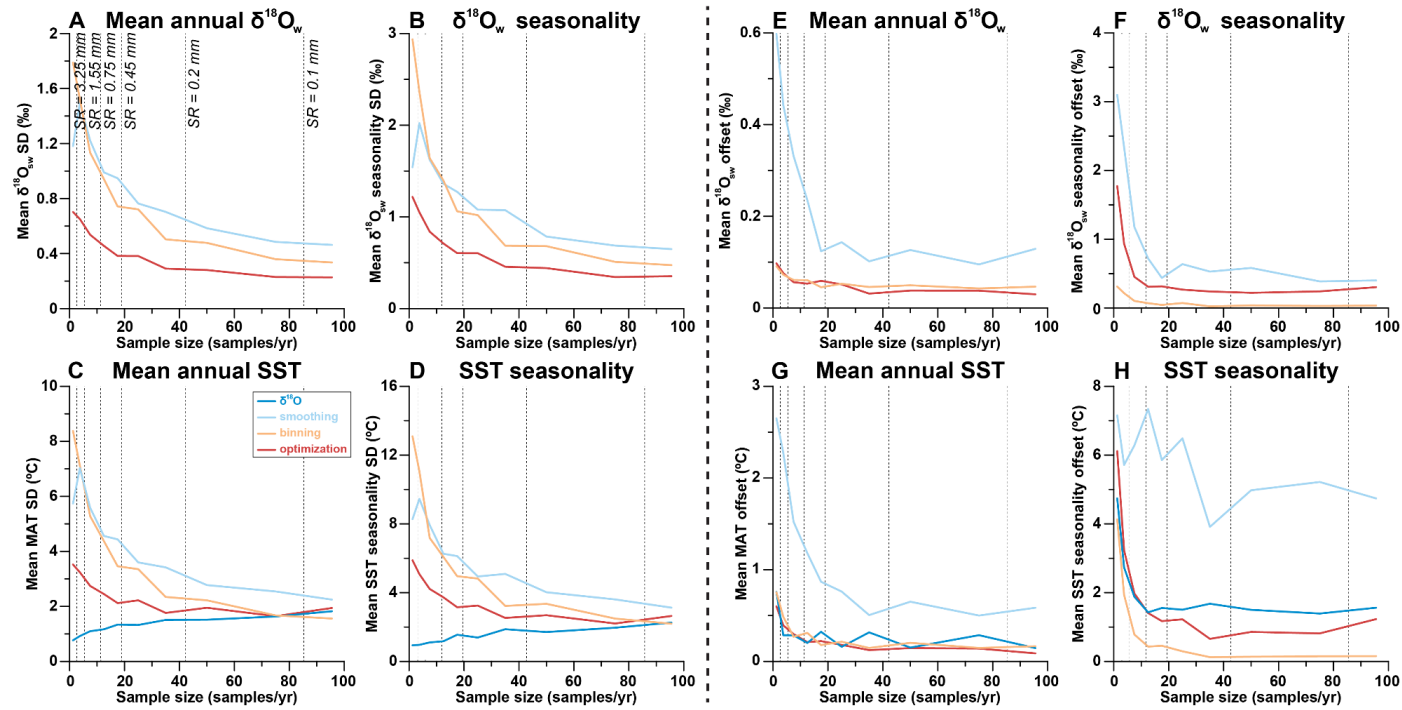
448 **Figure 8:** Overview of accuracy (absolute offset from “true” values) of reconstructions of mean annual  
 449 temperature (A), seasonal temperature range (B), mean annual  $\delta^{18}\text{O}_w$  (C) and seasonal range in  $\delta^{18}\text{O}_w$  (D),  
 450 with higher values (darker colors) indicating lower accuracy (higher offsets) based on average sampling  
 451 resolution (sampling interval of 0.45 mm). The different cases on the horizontal axis are color coded by  
 452 their difference from the control case (case 1; see legend on the right-hand side). Grey boxes indicate  
 453 cases for which reconstructions were not successful. All data on accuracy (difference between  
 454 reconstructed and “true” values) is provided in [Supplementary Data S4](#).

Formatted: Font: Italic



## Precision

## Accuracy

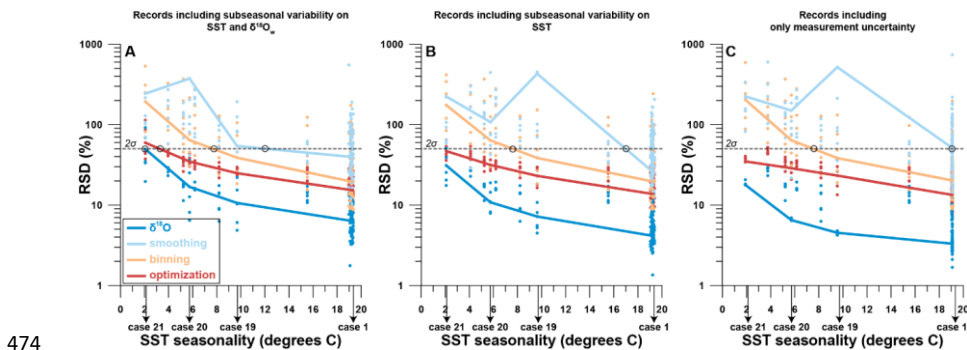


456

457 **Figure 9:** Effect of sampling resolution (in samples per year, see S5) on the precision (one standard deviation) of results of reconstructions of mean  
 458 annual  $\delta^{18}\text{O}_w$  (A), seasonal range in  $\delta^{18}\text{O}_w$  (B), mean annual SST (C) and seasonal range in SST (D). Effect on the accuracy (absolute offset from  
 459 actual value) of results of reconstructions of mean annual  $\delta^{18}\text{O}_w$  (E) and seasonal range in  $\delta^{18}\text{O}_w$  (F), mean annual SST (G) and seasonal range in  
 460 SST (H). Color coding follows the scheme in Fig. 1 and Fig. 4.

461 **3.3 Effect of sampling resolution**

462 As expected, increasing the temporal sampling resolution (i.e. number of samples per year) almost  
 463 invariably increases the precision and accuracy (**Fig. 9**) of reconstructions using all methods. An exception  
 464 to this rule is the precision of  $\delta^{18}\text{O}$  reconstructions, which decreases with increasing sampling resolution  
 465 (see **Fig. 9C-D**). Precision errors-standard deviations of all  $\Delta_{47}$ -based approaches eventually converge with  
 466 the initially much lower-higher precision error-of  $\delta^{18}\text{O}$  reconstructions when sampling resolution increases.  
 467 However, the sampling resolution required for  $\Delta_{47}$ -based reconstructions to rival or outcompete the  $\delta^{18}\text{O}$   
 468 reconstructions differs, with **optimization** requiring lower sampling resolutions than the other methods (e.g.  
 469 20-40 samples/year compared to 40-80 samples/year for **smoothing** and **binning**; **Fig. 9A-D**). Accuracy  
 470 also improves with sampling resolution (**Fig. 9E-H**). When grouping all cases together, it becomes clear  
 471 that  $\delta^{18}\text{O}$  reconstructions can only approach the accuracy of  $\Delta_{47}$ -based approaches for reconstructions of  
 472 MAT. Seasonality in both SST and  $\delta^{18}\text{O}_w$  is most accurately reconstructed using **binning**, and the  
 473 **smoothing** approach once again performs worst.



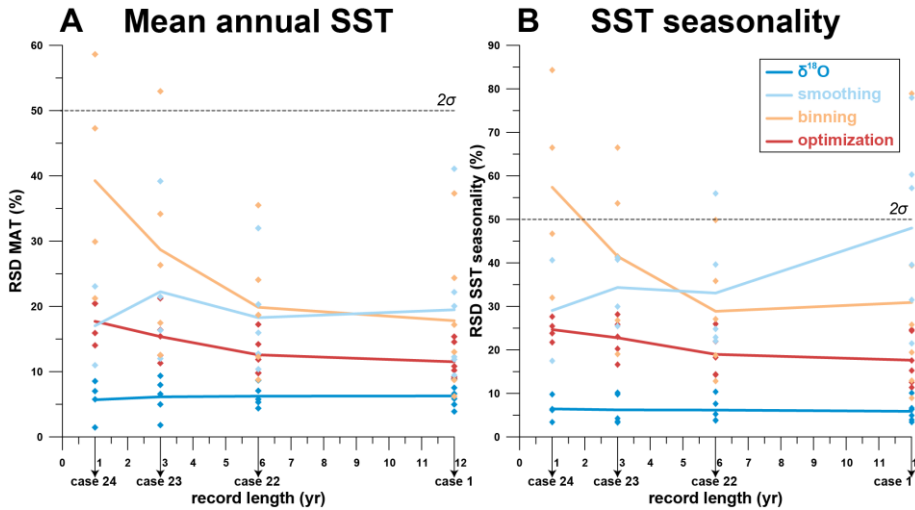
474 **Figure 10:** Effect of SST seasonality range (difference between warmest and coldest month) in the record  
 475 on the relative precision of SST seasonality reconstructions (“RSD”, defined as one standard deviation  
 476 divided by the mean value). **Panel A** shows precision results if random variability (“weather patterns”) in  
 477 both SST and  $\delta^{18}\text{O}_w$  as well as measurement uncertainty is added to the records (see **2.3.3** and **S1**). **Panel B**  
 478 shows precision of records with random variability in SST and measurement uncertainty only. **Panel C**  
 479 shows precision if only measurement uncertainty is considered. Color coding follows the scheme in **Fig. 1**  
 480 and **Fig. 4**. Shaded dots represent results at various sampling resolutions, while bold lines are averages  
 481 for all reconstruction approaches. Black circles highlight the places where curves cross the threshold of two  
 482 standard deviations, which indicates the minimum SST seasonality that can be resolved within 2 standard  
 483 deviations (~95% confidence level) using the reconstruction approach.

485

486 **3.4 Resolving SST seasonality**

487 Comparison of cases 19, 20 and 21 (SST seasonality of 9.7°C, 5.7°C and 2.1°C respectively) with control  
488 case 1 (SST seasonality of 19.3°C) shows how changes in the seasonal SST range affect the precision of  
489 measurements (**Fig. 10**; see also **Table 1** and [Supplementary Data S1](#)). The data reconfirms that  $\delta^{18}\text{O}$   
490 reconstructions are most precise; a deceptive statistic given the risk of highly inaccurate results this  
491 approach yields (see **Fig. 8**). Taking into consideration only analytical uncertainty, all approaches except  
492 for **smoothing** can confidently resolve at least the highest SST seasonality within a significance level of  
493 two standard deviations (~95%) using a moderate sampling resolution (mean of all resolutions shown in  
494 **Fig. 10**). Increasing sampling resolution improves the precision of  $\Delta_{47}$ -based reconstructions (see **Fig. 9D**),  
495 so high sampling resolutions (0.1 or 0.2 mm) allow smaller seasonal differences to be resolved. When  
496 random sub-annual variability is added to the SST and  $\delta^{18}\text{O}_w$  records (see **2.3.3**), the minimum seasonal  
497 SST extent that can be resolved decreases for all approaches (**Fig. 10B** and **10C**). Nevertheless,  $\delta^{18}\text{O}$  and  
498 **optimization** reconstructions remain able to resolve a relatively small SST seasonality of 2-4°C.

499



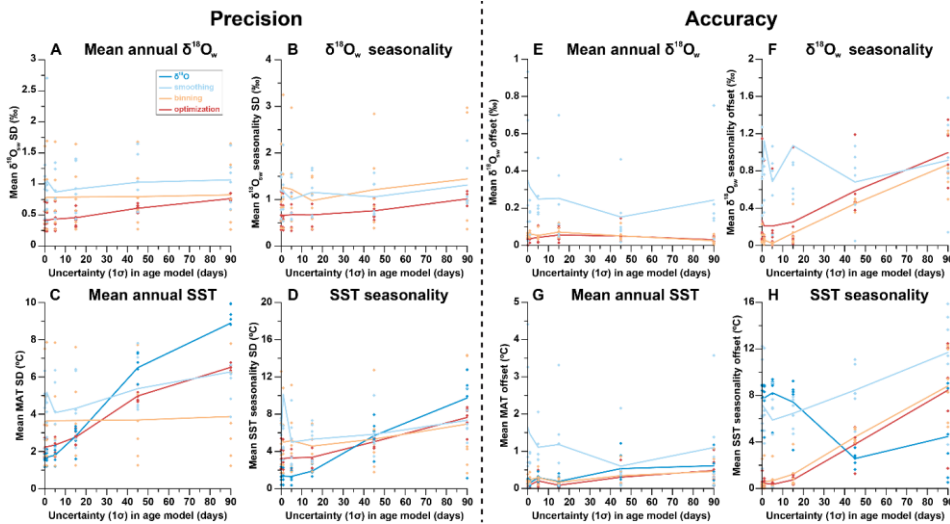
500  
 501 **Figure 11:** Effect of record length (in years) on the relative precision (one standard deviation as fraction of  
 502 the mean value) of results of reconstructions of mean annual SST (**A**) and SST seasonality (**B**). *Shaded*  
 503 *Colored* dots represent results for the six different sampling resolutions. Solid lines connect averages for  
 504 cases 1, 22, 23 and 24 for each reconstruction approach.

505

506 **3.5 Effect of record length**

507 The effect of variation in the length of the record was investigated by comparing cases 22, 23 and 24 (record  
 508 lengths of 6 years, 3 years and 1 year, respectively) with the control case (record length of 12 years; see  
 509 **Fig. 11** and **Table 1**). Precision of MAT and SST seasonality reconstructions slightly increase in larger  
 510 datasets (longer records) for **optimization** and **binning**, but not for **smoothing** and **δ<sup>18</sup>O** reconstructions.  
 511 Differences between reconstruction approaches remain relatively constant regardless of the length of the  
 512 record, with **general**-precision hierarchy **generally** remaining intact (**δ<sup>18</sup>O** > **optimization** > **binning** >  
 513 **smoothing**). However, in very short records (1-2 years) **smoothing** **generally** gains an advantage over  
 514 other  $\Delta_{47}$ -based methods due to its lack of sensitivity to changes in the record length, and **binning**  
 515 reconstructions are not precise enough to resolve MAT and SST seasonality within two standard deviations  
 516 (~95% confidence level). Variation in precision is largely driven by very **high-low** precision errors of  
 517 reconstructions in records with low sampling resolutions (sampling intervals of 1.55 mm or 3.25 mm; see

518 also Fig. 9A-D). As a result, most of the reduction in precision in shorter records can be mitigated by denser  
 519 sampling.



520  
 521 **Figure 12:** Effect of uncertainty in age model on the reproducibility-precision (standard deviation on  
 522 estimate) of results of reconstructions of mean annual  $\delta^{18}O_w$  (A) and seasonal range in  $\delta^{18}O_w$  (B), mean  
 523 annual SST (C) and seasonal range in SST (D). Effect of uncertainty in age model on the accuracy (offset  
 524 from true value) of results of reconstructions of mean annual  $\delta^{18}O_w$  (E) and seasonal range in  $\delta^{18}O_w$  (F),  
 525 mean annual SST (G) and seasonal range in SST (H). Color coding follows the scheme in Fig. 1 and Fig.  
 526 4.

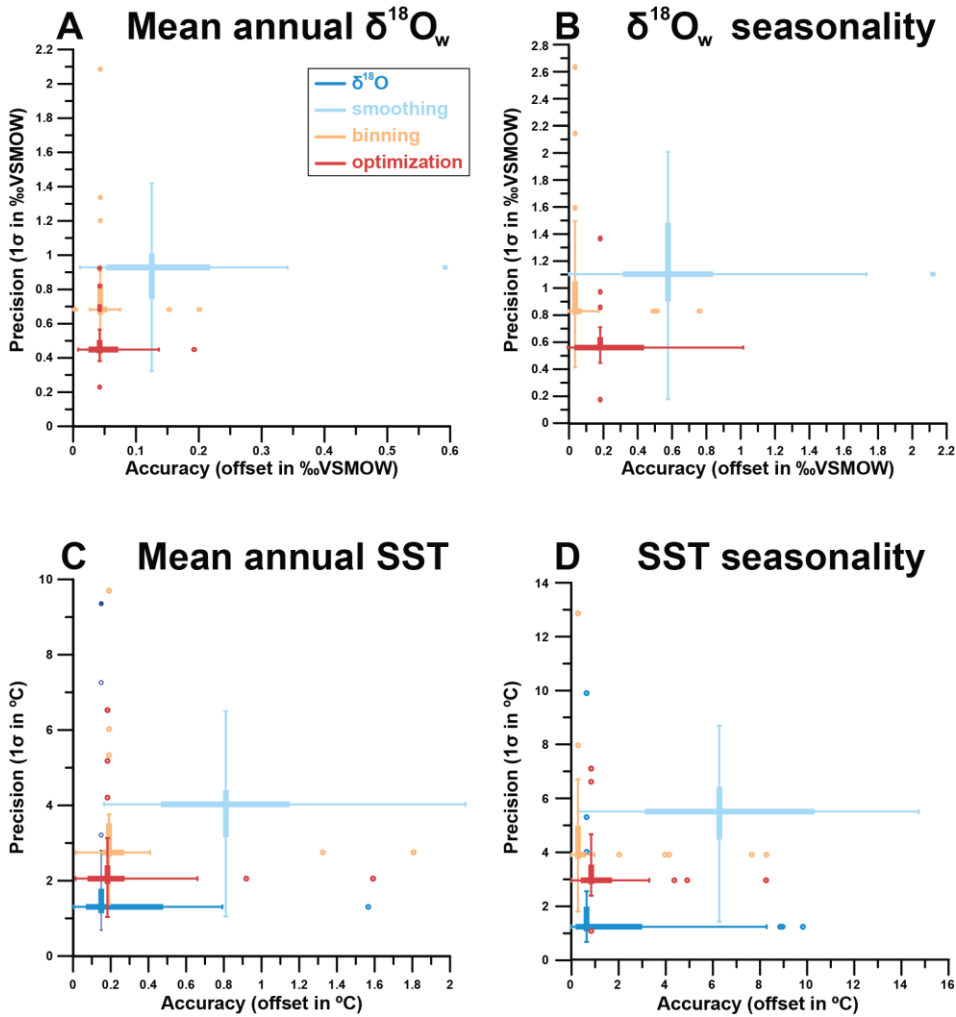
527

### 528 3.6 Effect of age model uncertainty

529 Uncertainty ~~on~~in the age model has a significant effect on both the precision and the accuracy (Fig. 12) of  
 530 reconstructions using all approaches. The  $\delta^{18}O$  reconstructions are most strongly affected by uncertainties  
 531 in the age model and suffer from a large decrease in precision with increasing age model uncertainty (Fig.  
 532 12C-D). The high reproducibility-precision of the  $\delta^{18}O$  approach in comparison with the  $\Delta_{47}$  approaches  
 533 quickly disappears when age model uncertainty increases beyond 20-30 days. Accuracy of  $\delta^{18}O_c$ -based  
 534 SST seasonality reconstructions initially improves with age model uncertainty (Fig. 12H). However, this  
 535 observation is likely caused by the fact that age model uncertainty was compared based on conditions in  
 536 case 9, which features a phase offset between SST and  $\delta^{18}O_w$  seasonality causing the  $\delta^{18}O$  method to be

Formatted: Justified, Line spacing: Double

537 highly inaccurate even without age model uncertainty. The precision of **smoothing** and **optimization**  
538 approaches also decreases with increasing age model uncertainty (**Fig 12A-D**), and the **optimization**  
539 approach loses its precision advantage over the **binning** and **smoothing** approaches when age model  
540 uncertainty increases beyond 30 days. The monthly **binning** approach is most resilient against increasing  
541 age model uncertainty. Seasonality reconstructions through both the **binning** and **optimization** approach  
542 quickly lose accuracy when age model uncertainty increases but the accuracy of the **smoothing** approach  
543 remains the worst of all  $\Delta_{47}$ -based approaches in regardless of age model uncertainty except in the case  
544 of  $\delta^{18}\text{O}_w$  seasonality at exceptionally high (>60 days) age uncertainty (**Fig. 12E-H**).



545  
 546 **Figure 13:** Overview of averages and ranges of accuracy (absolute offset from real value) and precision  
 547 (one standard deviation from the mean) on mean annual  $\delta^{18}\text{O}_w$  (A) and seasonal range in  $\delta^{18}\text{O}_w$  (B), mean  
 548 annual SST (C) and seasonal range in SST (D) within all cases using the four different reconstruction  
 549 approaches. Color coding follows the scheme in Fig. 1 and Fig. 4. Box-whisker plots for precision and  
 550 accuracy cross at their median values and outliers (colored symbols) are identified based on 2x the  
 551 interquartile difference (thick lines).  
 552

553 **4. Discussion**

554 **4.1 Performance of reconstruction approaches**

555 *4.1.1  $\delta^{18}O_c$  vs  $\Delta_{47}$ -based reconstructions*

556 **Figure 13** summarizes the general reliability of the four approaches.  $\delta^{18}O$  reconstructions are generally  
557 less accurate than  $\Delta_{47}$ -based reconstructions (especially **binning** and **optimization**; see also  
558 [Supplementary Data S9](#)). This is a consequence of the assumption that  $\delta^{18}O_w$  remains constant year-  
559 round, and that one knows its true value. Both these assumptions are problematic in the absence of  
560 independent evidence of the value of  $\delta^{18}O_w$ , especially in deep time settings (see e.g. Veizer and Prokoph,  
561 2015; Henkes et al., 2018). The risk of this assumption is made clear when comparing cases in which  $\delta^{18}O_w$   
562 is indeed constant year-round at the assumed value (0‰; e.g. cases 1-6 and 19-24) with cases in which  
563 shifts in  $\delta^{18}O_w$  occur, especially when these shifts are out of phase with respect to the SST seasonality (e.g.  
564 cases 9-11, 18 and 25-33; **Fig. 8C-D**). Cases mimicking or based on natural SST and SSS variability (cases  
565 14-18 and 30-33) as well as the modern oyster data (**Fig. 6**) yield stronger inaccuracies in MAT and  
566 seasonality reconstructions, showing that even in many modern natural circumstances the assumption of  
567 constant  $\delta^{18}O_w$  is problematic.

568 It is important to consider that the value of mean annual  $\delta^{18}O_w$  remained very close to the assumed value  
569 of 0‰ (within 0.15‰) in all cases except for natural data cases 30 (-1.55‰), 32 (1.01‰; see  
570 [Supplementary Data S5](#)) and the real oyster data (-1.42‰; **Fig. 5**). The SST values of these cases  
571 reconstructed using  $\delta^{18}O_c$  data show large offsets from their actual values (+6.7°C, -4.7°C and +10.3°C for  
572 case 30, case 32 and the real oyster data respectively; see **Fig. 6 and 8** and [Supplementary Data S5](#)).  
573 These offsets are equivalent to the temperature offset one might expect from inaccurately estimating  $\delta^{18}O_w$   
574 ( $\sim -4.6$  °C/‰; Kim and O'Neil, 1997) and are only rivaled by the offset in MAT reconstructions of case 18  
575 (+5.0°C), which has growth hiatuses obscuring the coldest half of the seasonal cycle. The fact that such  
576 differences in  $\delta^{18}O_w$  exist even in modern environments should not come as a surprise, given the available  
577 data on worldwide variability of  $\delta^{18}O_w$  (at least -3‰ to +2‰; e.g. LeGrande and Schmidt, 2006) and SSS  
578 (30 to 40; ESA, 2020) in modern ocean basins. However, it should warrant caution in using  $\delta^{18}O_c$  data for  
579 SST reconstructions even in modern settings. Implications for deep time reconstructions are even greater,



580 given the uncertainty on and variability in global average (let alone local)  $\delta^{18}\text{O}_w$  values (Jaffrés et al., 2007;  
581 Veizer and Prokoph, 2015). The complications of using  $\delta^{18}\text{O}_c$  as a proxy for marine temperatures in deep  
582 time are discussed in detail in O'Brien et al. (2017), and Tagliavento et al. (2019). Complications arising  
583 from variability in  $\delta^{18}\text{O}_w$  are more serious in climate records from euryhaline carbonate producers (e.g.  
584 oysters) than from stenohaline organisms (e.g. corals), as they are mainly driven by salinity fluctuations.  
585 For example, seasonal salinity variability in the North Sea in offshore sites away from freshwater sources  
586 can be as low as 0.25 (Harwood et al., 2008), compared to 3-4 in the coastal Texel site simulated in case  
587 30. Given this variability, studies using the  $\delta^{18}\text{O}_c$  proxy for SST reconstructions are recommended to either  
588 reconstruct  $\delta^{18}\text{O}_w$  through additional measurements (e.g. including clumped isotope analysis) or constrain  
589  $\delta^{18}\text{O}_w$  variability through isotope-enabled modelling (e.g. Williams et al., 2009)

590 The analytical uncertainty of individual  $\delta^{18}\text{O}_c$  aliquots (typically 1 S.D. of 0.05‰; e.g. de Winter et al., 2018)  
591 represents only ~1.1% of the variability in  $\delta^{18}\text{O}_c$  over the seasonal cycle (~4.3‰ for the default 20°C  
592 seasonality in case 1, following Kim and O'Neil, 1997). This is much smaller than the analytical uncertainty  
593 of  $\Delta_{47}$  (typically 1 S.D. of 0.02-0.04‰; e.g. Fernandez et al., 2018; de Winter et al., 2020b), which equates  
594 to 25-50% of the seasonal variability in  $\Delta_{47}$  (~0.08‰ for 20°C seasonality, following Bernasconi et al., 2018;  
595 see [Supplementary Data S7](#)). This roughly 20-fold difference in relative precision causes  $\delta^{18}\text{O}_c$  based SST  
596 reconstructions to be much more precise (see **Figs 7, 9-12**) than those based on  $\Delta_{47}$ , and forces the  
597 necessity for grouping  $\Delta_{47}$  data in reconstructions. However, as discussed above, the high precision of  $\delta^{18}\text{O}$   
598 reconstructions is a misleading statistic if they are highly inaccurate.

599 Our results show that paleoseasonality reconstructions based on  $\delta^{18}\text{O}_c$  can only be relied upon if there is  
600 strong independent evidence of the value of  $\delta^{18}\text{O}_w$  and if significant sub-annual variability in  $\delta^{18}\text{O}_w$  (>0.3‰,  
601 equivalent to a 2-3°C SST variability; see **Fig. 9-10**; Kim and O'Neil, 1997) can be excluded with confidence.  
602 Examples of such cases include fully marine environments unaffected by influxes of (isotopically light)  
603 freshwater or evaporation (increasing  $\delta^{18}\text{O}_w$ ; Rohling, 2013). Carbonate records from environments with  
604 more stable  $\delta^{18}\text{O}_w$  conditions include, for example, the *A. islandica* bivalves from considerable depth (30-  
605 50m) in the open marine Northern Atlantic (e.g. Schöne et al., 2005, on which case 33 is based). However,  
606 even here variability in  $\delta^{18}\text{O}_{sw}$  due to, for example, shifting influence of different bottom water masses

607 cannot be fully excluded. Previous reconstruction studies show that  $\delta^{18}\text{O}_w$  in smaller basins are heavily  
608 influenced by the processes affecting  $\delta^{18}\text{O}_w$  on smaller scales, such as local evaporation and freshwater  
609 influx from nearby rivers (e.g. Surge et al., 2001; Petersen et al., 2016). Consequently, accurate quantitative  
610 reconstructions of seasonal range in shallow marine environments with extreme seasonality may not be  
611 feasible using the  $\delta^{18}\text{O}$  approach, because these environments are invariably characterized by significant  
612 fluctuations in  $\delta^{18}\text{O}_w$  and growth rate.

613 While variability in  $\delta^{18}\text{O}_w$  compromises accurate  $\delta^{18}\text{O}$ -based seasonality reconstructions, the compilation  
614 in **Fig. 3** shows that its influence on the  $\delta^{18}\text{O}$  records is too small to affect the shape of the record to such  
615 a degree that seasonality is fully obscured. While natural situations with  $\delta^{18}\text{O}_w$  fluctuations large enough to  
616 totally counterbalance the effect of temperature seasonality on  $\delta^{18}\text{O}$  records are imaginable, these cases  
617 are likely rare. This means that chronologies based on  $\delta^{18}\text{O}$  seasonality, which are a useful tool to anchor  
618 seasonal variability in absence of independent growth markers (e.g. Judd et al., 2018; de Winter, 2021b),  
619 are reliable in most natural cases.

#### 620 4.1.2 Seasonality reconstructions using moving averages (*smoothing*)

621 Of the three methods for combining  $\Delta_{47}$  data, the **smoothing** approach clearly performs worst in all four  
622 reconstructed parameters (MAT, SST seasonality, mean annual  $\delta^{18}\text{O}_w$  and  $\delta^{18}\text{O}_w$  seasonality), both in  
623 terms of accuracy and precision (**Fig. 13**). While applying a moving average may be a good strategy for  
624 lowering the uncertainty of  $\Delta_{47}$ -based temperature reconstructions in a long time series (e.g. Rodríguez-  
625 Sanz et al., 2017), the method underperforms in cases where baseline and amplitude of a periodic  
626 component (e.g. MAT and SST seasonality) are extracted from a record. This is likely due to the smoothing  
627 effect of the moving average, which reduces the seasonal cycle and causes highly inaccurate seasonality  
628 reconstructions (offsets mounting to  $>6^\circ\text{C}$ ; **Fig. 13**). This bias is especially detrimental in cases where the  
629 seasonal cycle is obscured by seasonal growth halts (e.g. case 18), multi-annual trends in growth (e.g.  
630 case 4, 14 and 17) and multi-annual trends in SST (e.g. case 15 and 17; see **Fig. 7 and 8**). The poor  
631 performance of the **smoothing** approach can be slightly mitigated by increasing sampling resolution (**Fig**  
632 **9**), but even at high sampling resolutions (every 0.1 or 0.2 mm) the method still fails to reliably resolve  
633 seasonal SST ranges below  $5^\circ\text{C}$  even in idealized cases (case 19-21; **Fig. 10**). Increasing the number of

634 samples by analyzing longer records does not improve the result, because smoothing of the seasonal cycle  
635 by a moving average window introduces the same dampening bias if the temporal sampling resolution  
636 (number of samples per year) remains equal (**Fig. 11**).

637 More critically, employing the **smoothing** method may give the illusion that seasonality is more reduced,  
638 and severely bias reconstructions. This bias highlights the importance of using the official meteorological  
639 definition of seasonality as the difference between the averages of warmest and coldest month in  
640 paleoseasonality work (O'Donnell [et al. and Ignizio](#), 2012). This definition is much more robust than the  
641 “annual range” often cited based on maxima and minima in  $\delta^{18}\text{O}_c$  records. This “annual range” strongly  
642 depends on sampling resolution, which is typically  $<12$  samples/yr (Goodwin et al., 2003), equivalent to the  
643 third lowest sampling interval (0.75 mm) simulated in this study. Therefore, we strongly recommend future  
644 studies to adhere to the monthly definition of seasonality to foster comparison between studies. While inter-  
645 annual variability is lost by combining data from multiple years into monthly averages, this approach  
646 increases precision, accuracy and comparability of paleoseasonality results. Inter-annual variability can still  
647 be discussed from plots of raw data plotted in time or sampling domain.

#### 648 *4.1.3 Monthly binning, sample size optimization and age model uncertainty*

649 Overall, the most reliable paleoseasonality reconstructions can be obtained from either **binning** or  
650 **optimization** (**Fig. 13**). In general, **optimization** is slightly more precise, while **binning** yields more  
651 accurate estimates of seasonal range in SST and  $\delta^{18}\text{O}_w$  (**Fig. 13B and D**). The more flexible combination  
652 of aliquots in the **optimization** routine yields improved precision (especially on mean annual averages) in  
653 cases where parts of the record are undersampled or affected by hiatuses and simultaneous fluctuations  
654 in both SST and  $\delta^{18}\text{O}_w$  (e.g. case 3-6, 14-18, 30-33). The downside of this flexibility is that in the case of  
655 larger sample sizes, the seasonal variability may be dampened, like in the **smoothing** approach (see **4.1.2**).  
656 This apparent dampening effect may be reduced by allowing the sample size of summer and winter samples  
657 to vary independently in the **optimization** routine, at the cost of higher computational intensity due to the  
658 larger number of sample size combinations (see 2.1 and 4.2.2). The rigid grouping of data in monthly bins  
659 in **binning** prevents this dampening and therefore yields slightly more accurate estimates of seasonal  
660 ranges in SST and  $\delta^{18}\text{O}_w$ . A caveat of **binning** is that it requires a very reliable age model of the record, at

661 least on a monthly scale. If the age model has a large uncertainty, there is a risk that samples are grouped  
662 in the wrong month, which compromises the accuracy of **binning** reconstructions, especially for  
663 reconstructions of seasonal range (**Fig 12H**). This problem is exacerbated by potential phase shifts between  
664 seasonality in paleoclimate variables (SST and  $\delta^{18}\text{O}_w$ ) and calendar dates, which may occur in the presence  
665 of a reliable age model.

666 Previous authors attempted to circumvent the dating problem by analyzing high-resolution  $\delta^{18}\text{O}_c$  transects  
667 and subsequently sampling the seasonal extremes for clumped isotope analyses (Keating-Bitonti et al.,  
668 2011; Briard et al., 2020). While this approach does not require sub-annual age models, it has several  
669 disadvantages compared with the **binning** and **optimization** approaches: Firstly, it requires separate  
670 sampling for  $\delta^{18}\text{O}_c$  and  $\Delta_{47}$ , which may not be possible in high-resolution carbonate archives due to sample  
671 size limitations. Analyzing small aliquots for combined  $\delta^{18}\text{O}_c$  and  $\Delta_{47}$  analyses consumes less material.  
672 Secondly, individual summer and winter temperature reconstructions require large (> 1.5 mg; e.g.  
673 Fernandez et al., 2017)  $\Delta_{47}$  samples from seasonal extremes, which causes more time-averaging than the  
674 approaches combining small aliquots. Finally, the position of seasonal extremes estimated from the  $\delta^{18}\text{O}_c$   
675 record may not reflect the true seasonal extent if seasonal SST and  $\delta^{18}\text{O}_w$  cycles are not in phase (as in  
676 case 9), causing the seasonal  $\Delta_{47}$ -based SST reconstructions to underestimate the temperature  
677 seasonality. In such cases,  $\delta^{18}\text{O}_c$  and  $\Delta_{47}$  analyses on small aliquots allow the seasonality in SST and  $\delta^{18}\text{O}_w$   
678 to be disentangled, yielding more accurate seasonality reconstructions.

679 Techniques for establishing independent age models for climate archives range from counting of growth  
680 layers or increments (Schöne et al., 2008; Huyghe et al., 2019), modelling and extracting of rhythmic  
681 variability in climate proxies through statistical approaches (e.g. De Ridder et al., 2007; Goodwin et al.,  
682 2009; Judd et al., 2018; de Winter, 2021b) and interpolation of uncertainty on absolute dates (e.g. Scholz  
683 and Hoffman, 2011; Meyers, 2019; Sinnesael et al., 2019). While propagating uncertainty in the data on  
684 which age models are based onto the age model is relatively straightforward, errors on underlying *a priori*  
685 assumptions such as linear growth rate between dated intervals, (quasi-)sinusoidal forcing of climate cycles  
686 and the uncertainty on human-generated data such as layer counting are very difficult to quantify (e.g.  
687 Comboul et al., 2014) and may not be normally distributed. Results of cases 25-29 show that uncertainties

688 in the age domain can significantly compromise reconstructions (**Fig. 12**). Within the scope of this study,  
689 only the effect of symmetrical, normally distributed uncertainties on an artificial case with phase decoupled  
690 SST and  $\delta^{18}\text{O}_w$  seasonality (case 9) was tested. The effects of other types of uncertainties on the  
691 reconstructions remain unknown, highlighting an unknown uncertainty in paleoseasonality and other high-  
692 resolution paleoclimate studies that may introduce bias or lead to over-optimistic uncertainties on  
693 reconstructions. Future research could quantify this unknown uncertainty by propagating estimates of  
694 various types of uncertainty on depth values of samples and on the conversion from sampling to time  
695 domain in age models.

#### 696 **4.2 Conditions influencing success of reconstructions**

697 The reliability (accuracy and precision) of SST and  $\delta^{18}\text{O}_w$  reconstructions depend on case-specific  
698 conditions. The range of case studies tested in this study allowed us to evaluate the effect of variability in  
699 SST, growth rate,  $\delta^{18}\text{O}_w$ , sampling resolution and record length relative to the control case (case 1; see  
700 [Supplementary Data S1](#)). A summary of the effects of these changes is given in **Table 2**.

701

Variable	cases	Metric	Effect on reconstructions			
			$\delta^{18}\text{O}$	smoothing	binning	optimization
SST	12	Precision	0	+++	+	0
	15					
	17					
	19-21 30-33	Accuracy	+	+	0	+
Growth rate	2-6	Precision	+	++	++	+
	14-18					
	30-33	Accuracy	+	++	0	+
$\delta^{18}\text{O}_w$	7-11	Precision	+	++	0	0
	13-18					
	30-33	Accuracy	+++	+++	+	++
Sampling resolution	1-33	Precision	0	+++	++	++
		Accuracy	+	+	+++	+
Record length	22-24	Precision	0	0	+++	++
		Accuracy	+	0	++	++
Age model uncertainty?	25-29	Precision	+++	++	0	++
		Accuracy	+	+	++	++

702 **Table 2:** Qualitative summary of the effects of changes in variables relative from the ideal case on  
703 reconstructions using the four approaches. The “cases” column lists cases in which the changes in the  
704 respective variable relative to the control case (case 1) were represented (see **Table 1** and **S1**). “0” =  
705 negligible effect, “+” = weak increase in uncertainty, “++” = moderate increase in uncertainty, “+++” = strong  
706 increase in uncertainty. Precision and accuracy of all tests is given in **S9**.

707

#### 708 4.2.1 SST variability

709 Variability in water temperature most directly affects the proxies under study. By default (case 1), SST  
710 varies sinusoidally around a MAT of 20°C with an amplitude of 10°C (see 2.3.3, **Fig. 2** and **Supplementary**  
711 **Data S1**). In cases in which multi-annual variability in SST is simulated (e.g. case 15 and 17), the accuracy  
712 of SST reconstructions using  $\delta^{18}\text{O}$  and **optimization** are reduced, while the **binning** approach is less  
713 strongly affected. Examples of such multi-annual cyclicity are El-Niño Southern Oscillation (ENSO;  
714 Philander, 1983) or North Atlantic Oscillation (NOA; Hurrell, 1995). The effect is especially large in case 17,  
715 which simulates a tropical environment with reduced SST seasonality and a strong multi-annual cyclicity.  
716 This type of environment is analogous to the environment of tropical shallow water corals, which are often  
717 used as archives for ENSO variability (e.g. Charles et al., 1997; Fairbanks et al., 1997) and is similar to  
718 tropical cases from the Australian Great Barrier Reef (case 31) and Red Sea (case 32; see **Fig. 3**). We  
719 therefore recommend using the **binning** approach on carbonate records where multi-annual cyclicity is

720 prevalent and if a reliable age model can be established for these records (as in e.g. Sato, 1999; Scourse  
721 et al., 2006; Miyaji et al., 2010).

#### 722 4.2.2 Growth rate variability and hiatuses

723 **Figures 7 and 8** show that variations in the growth rate of records, including the occurrence of hiatuses,  
724 have a strong effect on reconstructions, especially using the **smoothing** approach. In general, hiatuses  
725 and slower growth reduce precision of monthly SST and  $\delta^{18}\text{O}_w$  reconstructions by reducing mean temporal  
726 sampling resolution (samples/yr; see **Fig. 9**), and because parts of the record are undersampled. The effect  
727 on accuracy depends strongly on the timing of changes in growth rate or the occurrence of hiatuses. Cases  
728 2-6 simulate specific growth rate effects and can be used to test these differences. The **smoothing** method  
729 is especially sensitive to changes in growth rate that take place in specific seasons, such as hiatuses in  
730 winter (case 2) or summer (case 3) and growth peaks in summer (case 5) or spring (case 6). The other  
731 reconstruction approaches are less affected by this bias, because they generally do not mix samples from  
732 different seasons. The  **$\delta^{18}\text{O}$**  method is especially well suited to deal with changes in growth rate because  
733 it does not require combining different aliquots for accurate SST reconstructions. The **binning** and  
734 **optimization** approaches are slightly less reliable in cases where growth rate decreases linearly or  
735 seasonally along the entire record (cases 4-6; **Fig. 2**). Because these two methods consider all samples in  
736 the records at once, they are more sensitive to changes in temporal sampling resolution along the record.  
737 It is worth noting that **optimization** is especially sensitive to sharp changes in growth rate in summer (e.g.  
738 cases 11, 14, 16 and 17) because those conditions force the **optimization** routine to use larger sample  
739 sizes or include samples outside the warmest month for summer temperature estimates. A potential solution  
740 to this problem could be to allow sample sizes of summer and winter groups to vary independently in the  
741 **optimization** routine (see 2.1). This would allow sample size in the undersampled season (in this case:  
742 summer) to become larger than that at the other end of the  $\delta^{18}\text{O}_c$  spectrum, reducing uncertainty on the  
743 more densely sampled season and therefore improving the entire seasonality reconstruction.

744 A worst-case scenario is represented by case 18, where the cold half of the year is not recorded. Such  
745 cases result in strong biases in reconstructions of mean annual and seasonal ranges in SST and  $\delta^{18}\text{O}_w$ ,  
746 regardless of which method is used. In such extreme cases the record simply contains insufficient

747 information to reconstruct variability in growth rate, SST and  $\delta^{18}\text{O}_w$ , and it seems that no statistical method  
748 would enable this missing information to be recovered. The solution for these reconstructions would be to  
749 establish reliable age models, independent of  $\delta^{18}\text{O}$  or  $\Delta_{47}$  data, which show that a large part of the seasonal  
750 cycle is missing. All methods used in this study rely on a conversion of SST and  $\delta^{18}\text{O}_w$  reconstructions to  
751 the time domain to define monthly time bins. This conversion breaks down in fossil examples when the  
752 seasonal cycle cannot be extracted from the archive, which happens when half of the seasonal cycle or  
753 more is obscured by growth hiatuses, as exemplified in case 18.

754 While hiatuses encompassing half of the seasonal cycle are uncommon, changes in growth rate are  
755 common in accretionary carbonate archives because conditions for (biotic or abiotic) carbonate  
756 mineralization often vary over time. This variability is either driven by biological constraints, such as  
757 senescence (e.g. Schöne, 2008; Hendriks et al., 2012), the reproductive cycle (Gaspar et al., 1999) or  
758 stress (Surge et al., 2001; Compton et al., 2007) or by variations in the environment that promote or inhibit  
759 carbonate production, such as seasonal variations in temperature (Crossland, 1984; Bahr et al., 2017) or  
760 precipitation (Dayem et al., 2010; Van Rampelbergh et al., 2014). In general, such conditions occur more  
761 frequently in mid- to high-latitude environments than in low-latitudes, and in more coastal environments  
762 rather than in open marine settings, because these environments contain stronger variations in the factors  
763 that influence growth rates (e.g. temperature, precipitation or freshwater influx; e.g. Surge et al., 2001;  
764 Ullmann et al., 2010). This difference was simulated in the cases representing natural variability (case 14-  
765 18 and 30-33). Accuracy in the coastal high-latitude settings (cases 16, 18 and 29) are indeed more strongly  
766 affected by changes in growth rate. Because in such highly variable environments growth rate variability  
767 often co-occurs with variability in  $\delta^{18}\text{O}_w$ , using  $\delta^{18}\text{O}_c$ -based reconstructions is not advised, unless  $\delta^{18}\text{O}_w$   
768 variability can be constrained or neglected (which is rare in these environments).

769 Additional complications include ~~that~~ the lack of constraint on growth rate variability because of  
770 uncertainties in the record's age model (see 4.1.3) and the effect of growth rate variability on the sampling  
771 resolution. The effect of growth rate on time-averaging within samples was not specifically tested in this  
772 study but introduces uncertainty in practice when archives with variable growth rate are sampled at a  
773 constant sampling resolution in the depth domain. In this case, parts of the archive with a lower growth rate



774 yield more time-averaged samples, potentially dampening one extreme of the seasonal cycle (e.g. Goodwin  
775 et al., 2003). In highly dynamic environments it is challenging to isolate all variables that introduce bias, and  
776 irregular variability in growth rate and  $\delta^{18}\text{O}_w$  will invariably introduce uncertainty in SST reconstructions,  
777 even when applying the best  $\Delta_{47}$ -based approaches (e.g. **binning** and **optimization**). In such examples,  
778 the results of natural variability cases (14-18 and 30-33) and of the real oyster data (**Fig. 6**) serve as  
779 benchmarks for the degree of uncertainty that may remain unexplained in these records.

#### 780 4.2.3 Variability in $\delta^{18}\text{O}_w$

781 As discussed in 4.1.1, these variations in  $\delta^{18}\text{O}_w$  have a large effect on the accuracy of  $\delta^{18}\text{O}_c$ -based  
782 reconstructions, and their occurrence constitutes the main advantage of applying the  $\Delta_{47}$  thermometer  
783 (Eiler, 2011). However, results of cases 7-11 in **Fig. 8** and **Table 2** show that  $\delta^{18}\text{O}_w$  variations can also bias  
784  $\Delta_{47}$ -based reconstructions, especially those of seasonal ranges and those using the **smoothing** approach.  
785 **Smoothing** reconstructions are biased by these  $\delta^{18}\text{O}_w$  shifts in much the same way as they are affected  
786 by shifts in growth rate (see 4.2.2). The **optimization** approach is sensitive to seasonal changes in  $\delta^{18}\text{O}_w$   
787 in antiphase with SST seasonality and by increases in  $\delta^{18}\text{O}_w$  in summer (e.g. due to excess evaporation;  
788 e.g. case 11), especially when used for reconstructions of  $\delta^{18}\text{O}_w$  seasonality. This effect arises because  
789 the **optimization** approach orders data based on  $\delta^{18}\text{O}_c$  and  $\Delta_{47}$  seasonality to isolate the  $\delta^{18}\text{O}_w$ -SST  
790 relationship. Both antiphase  $\delta^{18}\text{O}_w$  seasonality and summer evaporation dampen the seasonal  $\delta^{18}\text{O}_c$  cycle  
791 and therefore influences the reconstruction of the  $\delta^{18}\text{O}_w$ -SST relationship. A good example of this is seen  
792 in the real oyster data (**Fig. 6**), where  $\delta^{18}\text{O}_w$  and SST vary in phase and  $\delta^{18}\text{O}_w$  dampens the SST  
793 seasonality. The **binning** approach is more robust against  $\delta^{18}\text{O}_w$  variability that dampens the seasonal  
794 cycle and is therefore a better choice for absolute SST reconstructions in environments where summer  
795 evaporation or other  $\delta^{18}\text{O}_w$  variability in phase with SST seasonality is expected to occur, if the age model  
796 is reliable enough to allow monthly binning of raw data (see 4.1.3). Indeed, reconstructions from the  
797 lagoonal environment (case 16) and Red Sea case (case 32 which is characterized by strong summer  
798 evaporation; e.g. Titschack et al., 2010) show that **binning** is the most reliable choice in these  
799 environments.

#### 800 4.2.4 Variability in sampling resolution and record length

801 Other factors influencing the ~~effectivity~~ effectiveness of reconstructions are the sampling resolution and the  
802 length of the record. Many of the cases discussed in this study represent idealized cases with comparatively  
803 high sampling resolutions over comparatively long (12 yr) paleoseasonality records, which yield large  
804 sample sizes. By comparison, the typical age of mollusks, which are often used as paleoseasonality  
805 archives, is 2-5 years (Ivany, 2012). Records with the highest sampling resolutions (0.1 and 0.2 mm) contain  
806 up to 1200 samples. Generating such records is not impossible, but it is highly unlikely to be applied in  
807 paleoclimate studies given the limitation of resources (e.g. instrument time) and the desire to analyze  
808 multiple records from different specimens, species, localities or ages to gain a better understanding of the  
809 variability in paleoseasonality (e.g. Goodwin et al., 2003; Schöne et al., 2006; Petersen et al., 2016). In  
810 some cases large datasets are meticulously collected from single carbonate records (e.g. Schöne et al.,  
811 2005; Vansteenberghe et al., 2016; de Winter et al., 2020a; Shao et al., 2020). However, in such studies,  
812 the aim is often to investigate variability at a higher (e.g. daily; de Winter et al., 2020a) resolution or longer  
813 timescales (e.g. decadal to millennial; Schöne et al., 2005; Vansteenberghe et al., 2016; Shao et al., 2020)  
814 in addition to the seasonal cycle, rather than to improve the reliability of reconstructing one type of variability  
815 (e.g. seasonality) alone.

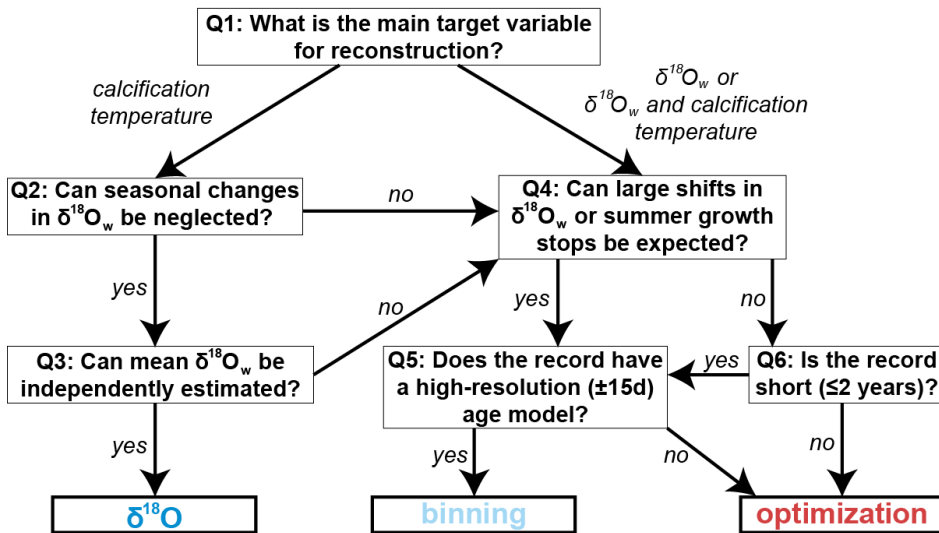
816 **Fig. 9** shows that increasing temporal sampling resolution (samples/yr) improves both the accuracy and  
817 precision of all  $\Delta_{47}$ -based reconstructions. This occurs because  $\Delta_{47}$  samples have a large analytical  
818 uncertainty (see **4.1.2**) and grouping of data therefore improves reconstructions. The decrease in precision  
819 of  $\delta^{18}\text{O}_c$ -based reconstructions (**Fig. 9C-D**) is explained by the fact that the analytical uncertainty of  $\delta^{18}\text{O}_c$   
820 measurements is much smaller than the variability introduced by natural sub-annual variability in SST and  
821  $\delta^{18}\text{O}_w$  unrelated to the seasonal cycle (see **Supplementary Data S4**). Therefore, higher sampling  
822 resolutions allow  $\delta^{18}\text{O}_c$  records to better capture this sub-seasonal variability, which introduces more noise  
823 ~~on to~~ the seasonal cycle (reducing precision) but causes monthly mean SST and  $\delta^{18}\text{O}_w$  to be more  
824 accurately reconstructed. Towards higher sampling resolutions, the gap in precision between  $\delta^{18}\text{O}_c$ - and  
825  $\Delta_{47}$ -based reconstructions closes, eventually (in an ideal case) diminishing the advantage of high analytical  
826 precision in  $\delta^{18}\text{O}_c$  measurements (**Fig. 9C-D**).

827 An optimum sample resolution can be defined for each method after which improving sampling resolution  
828 does not significantly improve the reliability of the reconstruction (as in de Winter et al., 2017). **Figure 9**  
829 shows that this optimum varies depending on which variable (MAT, SST seasonality, mean annual  $\delta^{18}\text{O}_w$   
830 or  $\delta^{18}\text{O}_w$  seasonality) is reconstructed. Therefore, **Fig. 9** will allow future researchers to determine the  
831 sampling resolution that is tailored to their purpose. In general, the improvement after a sample size of 20-  
832 30 samples per year is negligible for the **binning** and **optimization** methods if the total number of samples  
833 (depending on both sampling resolution and record length) is sufficient for monthly temperature  
834 reconstructions. Our data show that 200-250 paired  $\delta^{18}\text{O}_c$  and  $\Delta_{47}$  measurements are in general sufficient  
835 for a standard deviation of 2-3°C on monthly SST reconstructions using the **binning** or **optimization**  
836 approach, preferably when spread over multiple growth years to eliminate the effect of short-term weather  
837 events or years with exceptional seasonality (**Fig. 10**; **Supplementary Data S5**).

838 Record length only has a minimal influence on the **optimization** method but for very short records ( $\leq 2$   
839 years) **binning** becomes very imprecise, especially at low sampling resolutions (**Fig. 11**). The reason is  
840 that the sample size within monthly time bins becomes too small in these cases, while the more flexible  
841 sample size window of the optimization routine circumvents this problem. The choice between these two  
842 approaches should therefore be based on a tradeoff between the length of the record (in time) and the  
843 number of samples that can be retrieved from it. As a result, shorter-lived, fast-growing climate archives,  
844 such as large or fast-growing (e.g. juvenile) mollusk shells, are best sampled using a high temporal  
845 resolution ( $>30$  samples/yr) sampling strategy with the **optimization** approach. Longer lived archives with  
846 a lower mineralization rate, such as annually laminated speleothems, corals and gerontic mollusks, are  
847 best sampled using long time series at monthly resolution using the **binning** approach.

848 A simplified decision tree that could guide sampling strategies for future paleoseasonality studies is shown  
849 in **Figure 14**. Note that choices and tradeoffs for these reconstructions may differ depending on the archive  
850 and environment in which it formed (see discussion above).

## Schematic guide to reconstructing SST and $\delta^{18}\text{O}_w$ from accretionary carbonate archives



851  
 852 **Figure 15:** Schematic guide to choosing the right approach for reconstructing annual mean or seasonality  
 853 in SST and  $\delta^{18}\text{O}_w$  from accretionary carbonate archives. Recommendations are based on the results of  
 854 testing all four approaches on the entire range of cases. Researchers can follow the six steps (questions  
 855 Q1-6) to decide on the right approach for reconstructing the target variable. Guidelines are based on  
 856 *minimizing-maximizing* both accuracy and precision (see details in [Supplementary Data S9](#)). Note that the  
 857 *smoothing* approach is never the best choice. The choice between the two remaining  $\Delta_{47}$ -based  
 858 approaches (**binning** and **optimization**) relies heavily on the situation and may be driven by a preference  
 859 for more accurate or more precise results.

Formatted: Font: Italic

860

### 861 4.3 Implications for clumped isotope sample size

862 The **optimization** technique for grouping  $\Delta_{47}$  aliquots for accurate SST and  $\delta^{18}\text{O}_w$  reconstructions allows  
 863 us to assess the limitations of the clumped isotope thermometer for temperature reconstructions from high-  
 864 resolution carbonate archives. The optimal sample size given by the approach is different for different cases  
 865 and depends on the temporal sampling resolution and the characteristics of the record (see **S4**). As  
 866 expected, in cases more like the ideal case (case 1), optimal sample sizes are low (~14-24), while sample  
 867 sizes increase in more complicated cases based on simulated natural environments (case 14-18) or cases  
 868 based on actual SST and SSS data (cases 30-33). More confined SST seasonality (cases 19-21) also

869 requires larger samples to reconstruct (up to 100 samples in some cases). This is not surprising, because  
870 variability within samples will increase in records in which the seasonality is smaller or more obscured by  
871 other environmental variability. The optimal sample size between cases and sampling resolutions is not  
872 normally distributed but tails towards high sample sizes with some extreme outliers (Shapiro Wilk test  $p \ll$   
873 0.05; [Supplementary Data S10](#)). The median sample size of all our simulations is 17 aliquots. This number  
874 lies between the minimum number of 14 ~100  $\mu\text{g}$  replicates of standards calculated by Fernandez et al.  
875 (2017) and the minimum of 20-40 ~100  $\mu\text{g}$  aliquots required for optimal paleoseasonality reconstruction  
876 from fossil bivalves by de Winter et al. (2020b). This is to be expected since many of the cases explored in  
877 this study represent ideal cases compared with the natural situation. However, in these virtual cases a  
878 measure of random sub-annual variability in SST and  $\delta^{18}\text{O}_w$  was added (see [Fig. 4](#) and [Supplementary](#)  
879 [Data S2](#)), simulating a more realistic environment and resulting in poorer precision than replicates of a  
880 carbonate standard (as in Fernandez et al., 2017). Our simulations show that the optimum number of  
881 samples to be combined in seasonality studies depends on both the analytical uncertainty of  $\Delta_{47}$   
882 measurements (as represented by the estimate in Fernandez et al., 2017) and the variability between  
883 aliquots pooled within a sample that is attributed to actual variability within the record (as represented by  
884 our simulations and the estimate in de Winter et al., 2020b). The optimal sample size is therefore a good  
885 measure for the limitations of temperature variability that can be resolved in a record and can help  
886 researchers decide which strategy to apply for combining measurements to obtain the most reliable  
887 paleoseasonality estimates, or to decide whether extra sampling is required, even if the chosen approach  
888 is not to use the **optimization** routine itself. Note that the optimum sample size is kept equal for summer  
889 and winter samples in this study, and that the **optimization** approach can likely achieve better performance  
890 by considering unequal sample sizes in opposite seasons (see [4.1.3](#) and [4.2.2](#)). While this added flexibility  
891 comes at a higher computational cost due to the increased number of possible sample size combinations  
892 to be considered, future studies should investigate whether this updated **optimization** approach could yield  
893 more reliable seasonality reconstructions.

#### 894 4.4 Implications for other sample size problems

Formatted: Font: Bold

Formatted: Font: Bold

895 While the discussion above focuses on optimizing approaches for combining samples for clumped  
896 isotope analyses in paleoseasonality reconstructions, the problem of combining samples to reduce  
897 uncertainty and isolate variation in datasets is very common (e.g. Zhang et al., 2004; Merz and Thieken,  
898 2005; Tsukakoshi, 2011). Therefore, the approaches outlined and tested in this study have applications  
899 beyond paleoseasonality reconstructions. Examples of other problems that could benefit from applying  
900 similar approaches for reducing the uncertainty of estimates of target variables while minimizing the  
901 number of analyses required to meet analytical requirements include: (1) reconstructing  
902 paleoenvironmental variability in the terrestrial realm from tooth bioapatite (e.g. Passey and Cerling,  
903 2002; Kohn, 2004; Van Dam and Reichart, 2009; de Winter et al., 2016), (2) quantitative time series  
904 analysis of orbital cycles in stratigraphic records (e.g. Lourens et al., 2010; de Vleeschouwer et al., 2017;  
905 Noorbergen et al., [2017](#)[2018](#); Westerhold et al., 2020), (3) strontium isotope dating (e.g. McArthur et al.,  
906 2012; de Winter et al., 2020c), (4) reconstructing sub-seasonal variability from ultra-high-resolution  
907 records (e.g. from fast-growing mollusks and gastropods; e.g. Sano et al., 2012; Warter and Müller, 2017,  
908 de Winter et al., 2020d; Yan et al., 2020), and (5) reconstructing sea surface and deep-sea temperatures  
909 across short-lived (10–100 kyr) episodes of climate change or climate shifts from deep marine archives  
910 characterized by low sedimentation rates (e.g. Lear et al., 2008; Jenkyns, 2010; Stap et al., 2010;  
911 Lauretano et al., 2018). A more detailed discussion of the implications for other sample size problems is  
912 provided in the **Supplementary Information**.

913

914 **5. Conclusions and recommendations**

915 The performance of three  $\Delta_{47}$ -based approaches to reconstruct seasonality from accretionary carbonate  
916 archives was evaluated in comparison with conventional  $\delta^{18}\text{O}_c$ -based reconstructions in a wide range of  
917 case studies. From the results, we conclude that while  $\delta^{18}\text{O}_c$ -based reconstructions ( **$\delta^{18}\text{O}$** ) yield superior  
918 precision for SST reconstructions, this method runs a high risk of yielding inaccurate results due to innate  
919 assumptions about the value of  $\delta^{18}\text{O}_w$ , which must be estimated and assumed constant year-round. Unless  
920  $\delta^{18}\text{O}_w$  can be independently constrained or variability in  $\delta^{18}\text{O}_w$  can be neglected,  $\Delta_{47}$ -based reconstructions  
921 should be the method of choice for absolute mean annual temperature and SST seasonality  
922 reconstructions. Various techniques for combining  $\Delta_{47}$  data were evaluated. Our findings suggest that  
923 smoothing  $\Delta_{47}$  data using a moving average almost always ~~cases-results~~ in a dampening of the seasonal  
924 cycle which severely hampers recovery of seasonality. Applying the **smoothing** approach results in  
925 inaccuracies in reconstructions of MAT as well, especially in cases where part of the seasonal cycle is  
926 obscured by variability in growth rate or multi-annual trends. More reliable seasonality reconstructions are  
927 achieved with two approaches for combining  $\Delta_{47}$  data using time binning (**binning**) or applying a flexible  
928 sample size optimization (**optimization**) approach. Of these two approaches, **optimization** achieves better  
929 precision and can resolve smaller seasonal temperature differences with confidence. However, **binning** is  
930 often more accurate, and outperforms **optimization** as the most reliable approach. This is especially true  
931 in cases with growth stops or  $\delta^{18}\text{O}_w$  changes in phase with temperature seasonality (e.g. strong seasonal  
932 evaporation or freshwater influx) and in longer multi-annual time series with a reliable age model.  
933 **Optimization** is the better choice for shorter (<3 years) records, especially if the sampling resolution can  
934 be increased, such as in short, fast growing climate archives.

935 Despite the focus on the problem of resolving seasonality in carbonate archives, the findings in this study  
936 have applications for other problems in earth science where sample size and sampling resolution put limits  
937 on the ability to resolve specific trends, events, and cycles from time series. While the above-mentioned  
938 recommendations of the **optimization** and **binning** methods are likely valid for most studies aiming to  
939 quantify the mean and amplitude of a specific cycle or event (equivalent to MAT and SST seasonality),

940 (dynamic) moving averages (**smoothing**) are expected to yield the best results in studies quantifying  
941 aperiodic trends from longer data series.

942

#### 943 **Code availability**

944 All scripts used to make the calculations described in this study are compiled in the documented R package  
945 “seasonalclumped”, which is freely available on the open-source online R-database CRAN (de Winter,  
946 2021a; <https://cran.r-project.org/web/packages/seasonalclumped>). Annotated R scripts used to make  
947 calculations for this study are available in the digital supplement uploaded to the open-source online  
948 repository Zenodo ([www.doi.org/10.5281/zenodo.3899926](http://www.doi.org/10.5281/zenodo.3899926)).

949

#### 950 **Data availability**

951 Supplementary data, figures and tables as well as all scripts used to do the calculations and create the  
952 virtual datasets used in this study are deposited in the open-source online repository Zenodo  
953 ([www.doi.org/10.5281/zenodo.3899926](http://www.doi.org/10.5281/zenodo.3899926)). Virtual datasets generated within the context of this study are also  
954 made available as datafiles within the R package that contains the scripts used for this study  
955 (“seasonalclumped”; de Winter, 2021a; see <https://cran.r-project.org/web/packages/seasonalclumped>).

956

#### 957 **Author contributions**

958 NJW designed the study, wrote the scripts for all calculations, and created a first draft of the manuscript  
959 text and figures. MZ, TA and NJW worked together from the first draft towards the final manuscript. All  
960 authors contributed to the representation of the data and methods in figures and to the discussion of the  
961 implications of the data in the discussion.

962

#### 963 **Competing Interests**



964 The authors have no potential conflicts of interest to declare with regards to this study.

965

#### 966 **Acknowledgements**

967 The authors would like to thank [editor Alberto Reyes for his helpful suggestions for improving the](#)  
968 [manuscript and for moderating the review process. Thanks to Andrew Johnson and two anonymous](#)  
969 [reviewers for their comments which helped improve the manuscript.](#) ~~a~~All members of the Clumped Isotope  
970 research group of Utrecht University, most notably Ilja Kocken and dr. Inigo Müller, [are acknowledged](#) for  
971 their comments and recommendations on a presentation of the initial results of this study.

972

#### 973 **Financial support**

974 NJW is funded by the European Commission through a Marie Skłodowska Curie Individual Fellowship  
975 (UNBIAS, grant # 843011) and by the Flemish Research Council (FWO) through a Junior Postdoctoral  
976 Fellowship (12ZB220N).

977

#### 978 **References**

979 Bahr, K. D., Jokieli, P. L. and Rodgers, K. S.: Seasonal and annual calcification rates of the Hawaiian reef  
980 coral, *Montipora capitata*, under present and future climate change scenarios, *ICES J Mar Sci*, 74(4),  
981 1083–1091, <https://doi.org/10.1093/icesjms/fsw078>, 2017.

982 Bernasconi, S. M., Müller, I. A., Bergmann, K. D., Breitenbach, S. F., Fernandez, A., Hodell, D. A., Jaggi,  
983 M., Meckler, A. N., Millan, I. and Ziegler, M.: Reducing uncertainties in carbonate clumped isotope  
984 analysis through consistent carbonate-based standardization, *Geochemistry, Geophysics, Geosystems*,  
985 19(9), 2895–2914, 2018.

986 Brand, W. A., Coplen, T. B., Vogl, J., Rosner, M. and Prohaska, T.: Assessment of international reference  
987 materials for isotope-ratio analysis (IUPAC Technical Report), *Pure and Applied Chemistry*, 86(3), 425–  
988 467, <https://doi.org/10.1515/pac-2013-1023>, 2014.

989 Briard, J., Pucéat, E., Vennin, E., Daëron, M., Chavagnac, V., Jaillet, R., Merle, D. and de Rafélis, M.:  
990 Seawater paleotemperature and paleosalinity evolution in neritic environments of the Mediterranean  
991 margin: Insights from isotope analysis of bivalve shells, *Palaeogeography, Palaeoclimatology,*  
992 *Palaeoecology*, 543, 109582, <https://doi.org/10.1016/j.palaeo.2019.109582>, 2020.

- 993 [Bowen, G.J. WaterIsotopes.org: http://wateriso.utah.edu/waterisotopes/index.html](http://wateriso.utah.edu/waterisotopes/index.html), last access: 28 July  
994 [2020](http://doi.org/10.1016/j.gca.2020.11.019).
- 995 Caldarescu, D. E., Sadatzki, H., Andersson, C., Schäfer, P., Fortunato, H. and Meckler, A. N.: Clumped  
996 isotope thermometry in bivalve shells: A tool for reconstructing seasonal upwelling, *Geochimica et*  
997 *Cosmochimica Acta*, 294, 174–191, <https://doi.org/10.1016/j.gca.2020.11.019>, 2021.
- 998 Charles, C. D., Hunter, D. E. and Fairbanks, R. G.: Interaction between the ENSO and the Asian monsoon  
999 in a coral record of tropical climate, *Science*, 277(5328), 925–928, 1997.
- 1000 Comboul, M., Emile-Geay, J., Evans, M. N., Mirnateghi, N., Cobb, K. M. and Thompson, D. M.: A  
1001 probabilistic model of chronological errors in layer-counted climate proxies: applications to annually  
1002 banded coral archives, *Climate of the Past*, 10(2), 825–841, 2014.
- 1003 Compton, T. J., Rijkenberg, M. J. A., Drent, J. and Piersma, T.: Thermal tolerance ranges and climate  
1004 variability: A comparison between bivalves from differing climates, *Journal of Experimental Marine*  
1005 *Biology and Ecology*, 352(1), 200–211, <https://doi.org/10.1016/j.jembe.2007.07.010>, 2007.
- 1006 Cook, E. R. and Kairiukstis, L. A.: *Methods of dendrochronology: applications in the environmental*  
1007 *sciences*, Springer Science & Business Media., 2013.
- 1008 Cramer, B. S., Toggweiler, J. R., Wright, J. D., Katz, M. E. and Miller, K. G.: Ocean overturning since the  
1009 Late Cretaceous: Inferences from a new benthic foraminiferal isotope compilation, *Paleoceanography*,  
1010 24(4), <https://doi.org/10.1029/2008PA001683>, 2009.
- 1011 Crossland, C.: Seasonal variations in the rates of calcification and productivity in the coral *Acropora formosa*  
1012 on a high-latitude reef, *Marine Ecology Progress Series*, 15, 135–140,  
1013 <https://doi.org/10.3354/meps015135>, 1984.
- ~~1014 van Dam, J. A. and Reichart, G. J.: Oxygen and carbon isotope signatures in late Neogene horse teeth~~  
~~1015 ~~from Spain and application as temperature and seasonality proxies, *Palaeogeography,*~~~~  
~~1016 ~~*Palaeoclimatology, Palaeoecology*, 274(1–2), 64–81, <https://doi.org/10.1016/j.palaeo.2008.12.022>,~~~~  
~~1017 ~~2009.~~~~
- 1018 Dattalo, P.: *Determining Sample Size: Balancing Power, Precision, and Practicality*, Oxford University  
1019 Press, USA., 2008.
- 1020 Dayem, K. E., Molnar, P., Battisti, D. S. and Roe, G. H.: Lessons learned from oxygen isotopes in modern  
1021 precipitation applied to interpretation of speleothem records of paleoclimate from eastern Asia, *Earth and*  
1022 *Planetary Science Letters*, 295(1–2), 219–230, 2010.
- 1023 De Ridder, F., de Brauwere, A., Pintelon, R., Schoukens, J., Dehairs, F., Baeyens, W. and Wilkinson, B.  
1024 H.: Comment on: Paleoclimatic inference from stable isotope profiles of accretionary biogenic hardparts—  
1025 a quantitative approach to the evaluation of incomplete data, by Wilkinson, B.H., Ivany, L.C., 2002.  
1026 *Palaeogeogr. Palaeoclimatol. Palaeoecol.* 185, 95–114, *Palaeogeography, Palaeoclimatology, Palaeoecology*,  
1027 248(3–4), 473–476, <https://doi.org/10.1016/j.palaeo.2006.08.004>, 2007.
- 1028 De Vleeschouwer, D., Vahlenkamp, M., Crucifix, M. and Pälike, H.: Alternating Southern and Northern  
1029 Hemisphere climate response to astronomical forcing during the past 35 my, *Geology*, 45(4), 375–378,  
1030 2017.
- 1031 de Winter, N. J., Snoeck, C. and Claeys, P.: Seasonal Cyclicity in Trace Elements and Stable Isotopes of  
1032 Modern Horse Enamel, *PLoS one*, 11(11), e0166678, 2016.

- 1033 de Winter, N., Sinnesael, M., Makarona, C., Vansteenberge, S. and Claeys, P.: Trace element analyses of  
 1034 carbonates using portable and micro-X-ray fluorescence: Performance and optimization of measurement  
 1035 parameters and strategies., *Journal of Analytical Atomic Spectrometry*, 32(6), 1211–1223,  
 1036 <https://doi.org/10.1039/C6JA00361C>, 2017.
- 1037 de Winter, N. J., Vellekoop, J., Vorsselmans, R., Golreihan, A., Soete, J., Petersen, S. V., Meyer, K. W.,  
 1038 Casadio, S., Speijer, R. P. and Claeys, P.: An assessment of latest Cretaceous *Pycnodonte vesicularis*  
 1039 (Lamarck, 1806) shells as records for palaeoseasonality: a multi-proxy investigation, *Climate of the Past*,  
 1040 14(6), 725–749, 2018.
- 1041 ~~de Winter, N. J., Goderis, S., Malderen, S. J. M. V., Sinnesael, M., Vansteenberge, S., Snoeck, C., Belza,~~  
 1042 ~~J., Vanhaecke, F. and Claeys, P.: Subdaily-Scale Chemical Variability in a *Torreites Sanchezi* Rudist~~  
 1043 ~~Shell: Implications for Rudist Paleobiology and the Cretaceous Day-Night Cycle, *Paleoceanography and*~~  
 1044 ~~*Paleoclimatology*, 35(2), e2019PA003723, <https://doi.org/10.1029/2019PA003723>, 2020a.~~
- 1045 de Winter, N. J., Müller, I. A., Kocken, I. J., Thibault, N., Ullmann, C. V., Farnsworth, A., Lunt, D. J., Claeys,  
 1046 P. and Ziegler, M.: First absolute seasonal temperature estimates for greenhouse climate from clumped  
 1047 isotopes in bivalve shells, *Nature Communications*, in review, <https://doi.org/10.21203/rs.3.rs-39203/v1>,  
 1048 [2020a](https://doi.org/10.21203/rs.3.rs-39203/v1)[2020b](https://doi.org/10.21203/rs.3.rs-39203/v1).
- 1049 de Winter, N. J., Ullmann, C. V., Sørensen, A. M., Thibault, N., Goderis, S., Van Malderen, S. J. M., Snoeck,  
 1050 C., Goolaerts, S., Vanhaecke, F. and Claeys, P.: Shell chemistry of the boreal Campanian bivalve  
 1051 ~~&lt;i>&lt;i>Rastellum diluvianum&lt;/i>&lt;/i>~~ (Linnaeus, 1767) reveals temperature seasonality, growth rates  
 1052 and life cycle of an extinct Cretaceous oyster, *Biogeosciences*, 17(11), 2897–2922,  
 1053 <https://doi.org/10.5194/bg-17-2897-2020>, [2020b](https://doi.org/10.5194/bg-17-2897-2020)[2020c](https://doi.org/10.5194/bg-17-2897-2020).
- 1054 ~~de Winter, N. J., Goderis, S., Malderen, S. J. M. V., Sinnesael, M., Vansteenberge, S., Snoeck, C., Belza,~~  
 1055 ~~J., Vanhaecke, F. and Claeys, P.: Subdaily-Scale Chemical Variability in a *Torreites Sanchezi* Rudist~~  
 1056 ~~Shell: Implications for Rudist Paleobiology and the Cretaceous Day-Night Cycle, *Paleoceanography and*~~  
 1057 ~~*Paleoclimatology*, 35(2), e2019PA003723, <https://doi.org/10.1029/2019PA003723>, 2020c.~~
- 1058 de Winter, N. J., Vellekoop, J., Clark, A. J., Stassen, P., Speijer, R. P. and Claeys, P.: The giant marine  
 1059 gastropod *Campanile giganteum* (Lamarck, 1804) as a high-resolution archive of seasonality in the  
 1060 Eocene greenhouse world, *Geochemistry, Geophysics, Geosystems*, 21(n/a), e2019GC008794,  
 1061 <https://doi.org/10.1029/2019GC008794>, 2020d.
- 1062 de Winter, N. J.: seasonalclumped: Toolbox for Clumped Isotope Seasonality Reconstructions.  
 1063 <https://CRAN.R-project.org/package=seasonalclumped>, last access: 4 February 2021, 2021 a.
- 1064 de Winter, N. J.: ShellChron 0.2.8: A new tool for constructing chronologies in accretionary carbonate  
 1065 archives from stable oxygen isotope profiles, *Geoscientific Model Development Discussions*, 1–37,  
 1066 <https://doi.org/10.5194/gmd-2020-401>, 2021b.
- 1067 Denton, G. H., Alley, R. B., Comer, G. C. and Broecker, W. S.: The role of seasonality in abrupt climate  
 1068 change, *Quaternary Science Reviews*, 24(10), 1159–1182,  
 1069 <https://doi.org/10.1016/j.quascirev.2004.12.002>, 2005.
- 1070 ~~Eiler, J. M.: *Paleoclimate reconstruction using carbonate clumped isotope thermometry*, 30, 3575–3588,~~  
 1071 ~~2011.~~
- 1072 Fairbanks, R. G., Evans, M. N., Rubenstone, J. L., Mortlock, R. A., Broad, K., Moore, M. D. and Charles,  
 1073 C. D.: Evaluating climate indices and their geochemical proxies measured in corals, *Coral Reefs*, 16(1),  
 1074 S93–S100, <https://doi.org/10.1007/s003380050245>, 1997.

Formatted: Font: Italic

- 1075 Fernandez, A., Müller, I. A., Rodríguez-Sanz, L., van Dijk, J., Looser, N. and Bernasconi, S. M.: A  
 1076 reassessment of the precision of carbonate clumped isotope measurements: implications for calibrations  
 1077 and paleoclimate reconstructions, *Geochemistry, Geophysics, Geosystems*, 18(12), 4375–4386, 2017.
- 1078 Gaspar, M. B., Ferreira, R. and Monteiro, C. C.: Growth and reproductive cycle of *Donax trunculus* L.,  
 1079 (Mollusca: Bivalvia) off Faro, southern Portugal, *Fisheries Research*, 41(3), 309–316,  
 1080 [https://doi.org/10.1016/S0165-7836\(99\)00017-X](https://doi.org/10.1016/S0165-7836(99)00017-X), 1999.
- 1081 Goodwin, D. H., Schöne, B. R. and Dettman, D. L.: Resolution and fidelity of oxygen isotopes as  
 1082 paleotemperature proxies in bivalve mollusk shells: models and observations, *Palaios*, 18(2), 110–125,  
 1083 2003.
- 1084 Goodwin, D. H., Paul, P. and Wissink, C. L.: MoGroFunGen: A numerical model for reconstructing intra-  
 1085 annual growth rates of bivalve molluscs, *Palaeogeography, Palaeoclimatology, Palaeoecology*, 276(1),  
 1086 47–55, <https://doi.org/10.1016/j.palaeo.2009.02.026>, 2009.
- 1087 Harwood, A. J. P., Dennis, P. F., Marca, A. D., Pilling, G. M. and Millner, R. S.: The oxygen isotope  
 1088 composition of water masses within the North Sea, *Estuarine, Coastal and Shelf Science*, 78(2), 353–  
 1089 359, <https://doi.org/10.1016/j.ecss.2007.12.010>, 2008.
- 1090 Hendriks, I. E., Basso, L., Deudero, S., Cabanellas-Reboredo, M. and Álvarez, E.: Relative growth rates of  
 1091 the noble pen shell *Pinna nobilis* throughout ontogeny around the Balearic Islands (Western  
 1092 Mediterranean, Spain), *Journal of Shellfish Research*, 31(3), 749–756, 2012.
- 1093 Henkes, G. A., Passey, B. H., Grossman, E. L., Shenton, B. J., Yancey, T. E. and Pérez-Huerta, A.:  
 1094 Temperature evolution and the oxygen isotope composition of Phanerozoic oceans from carbonate  
 1095 clumped isotope thermometry, *Earth and Planetary Science Letters*, 490, 40–50,  
 1096 <https://doi.org/10.1016/j.epsl.2018.02.001>, 2018.
- 1097 Hurrell, J. W.: Decadal trends in the North Atlantic Oscillation: regional temperatures and precipitation,  
 1098 *Science*, 269(5224), 676–679, 1995.
- 1099 Huybers, P. and Curry, W.: Links between annual, Milankovitch and continuum temperature variability,  
 1100 *Nature*, 441(7091), 329, 2006.
- 1101 Huyghe, D., Lartaud, F., Emmanuel, L., Merle, D. and Renard, M.: Palaeogene climate evolution in the  
 1102 Paris Basin from oxygen stable isotope ( $\delta^{18}\text{O}$ ) compositions of marine molluscs, *Journal of the*  
 1103 *Geological Society*, 172(5), 576–587, 2015.
- 1104 Huyghe, D., de Rafélis, M., Ropert, M., Mouchi, V., Emmanuel, L., Renard, M. and Lartaud, F.: New insights  
 1105 into oyster high-resolution hinge growth patterns, *Marine biology*, 166(4), 48, 2019.
- 1106 IPCC: IPCC, 2013: Climate Change 2013: The Physical Science Basis. Contribution of Working Group I to  
 1107 the Fifth Assessment Report of the Intergovernmental Panel on Climate Change, 1535 pp, Cambridge  
 1108 Univ. Press, Cambridge, UK, and New York., 2013.
- 1109 Ivany, L. C.: Reconstructing paleoseasonality from accretionary skeletal carbonates—challenges and  
 1110 opportunities, *The Paleontological Society Papers*, 18, 133–166, 2012.
- 1111 [Jaffrés, J. B. D., Shields, G. A., and Wallmann, K.: The oxygen isotope evolution of seawater: A critical](https://doi.org/10.1016/j.earscirev.2007.04.002)  
 1112 [review of a long-standing controversy and an improved geological water cycle model for the past 3.4](https://doi.org/10.1016/j.earscirev.2007.04.002)  
 1113 [billion years, \*Earth-Science Reviews\*, 83, 83–122, <https://doi.org/10.1016/j.earscirev.2007.04.002>, 2007.](https://doi.org/10.1016/j.earscirev.2007.04.002)

1114 Jenkyns, H. C.: Geochemistry of oceanic anoxic events, *Geochemistry, Geophysics, Geosystems*, 11(3),  
1115 <https://doi.org/10.1029/2009GC002788>, 2010.

1116 *Johnson, A. L. A., Valentine, A. M., Leng, M. J., Schöne, B. R., and Sloane, H. J.: Life history, environment*  
1117 *and extinction of the scallop *Carolinapecten eboreus* (Conrad) In the Plio-Pleistocene of the U.S. eastern*  
1118 *seaboard, PALAIOS, 34, 49–70, <https://doi.org/10.2110/palo.2018.056>, 2019.*

Formatted: Font: Italic

1119 Jones, A. M., Iacumin, P. and Young, E. D.: High-resolution  $\delta^{18}\text{O}$  analysis of tooth enamel phosphate by  
1120 isotope ratio monitoring gas chromatography mass spectrometry and ultraviolet laser fluorination, , 8,  
1121 1999.

1122 Judd, E. J., Wilkinson, B. H. and Ivany, L. C.: The life and time of clams: Derivation of intra-annual growth  
1123 rates from high-resolution oxygen isotope profiles, *Palaeogeography, Palaeoclimatology, Palaeoecology*,  
1124 490, 70–83, 2018.

1125 Keating-Bitonti, C. R., Ivany, L. C., Affek, H. P., Douglas, P. and Samson, S. D.: Warm, not super-hot,  
1126 temperatures in the early Eocene subtropics, *Geology*, 39(8), 771–774,  
1127 <https://doi.org/10.1130/G32054.1>, 2011.

1128 Kele, S., Breitenbach, S. F., Capezzuoli, E., Meckler, A. N., Ziegler, M., Millan, I. M., Kluge, T., Deák, J.,  
1129 Hanselmann, K. and John, C. M.: Temperature dependence of oxygen-and clumped isotope fractionation  
1130 in carbonates: a study of travertines and tufas in the 6–95 C temperature range, *Geochimica et*  
1131 *Cosmochimica Acta*, 168, 172–192, 2015.

1132 Kim, S.-T. and O’Neil, J. R.: Equilibrium and nonequilibrium oxygen isotope effects in synthetic carbonates,  
1133 *Geochimica et Cosmochimica Acta*, 61(16), 3461–3475, [https://doi.org/10.1016/S0016-7037\(97\)00169-](https://doi.org/10.1016/S0016-7037(97)00169-5)  
1134 5, 1997.

1135 Kocken, I. J., Müller, I. A. and Ziegler, M.: Optimizing the Use of Carbonate Standards to Minimize  
1136 Uncertainties in Clumped Isotope Data, *Geochemistry, Geophysics, Geosystems*, 20(11), 5565–5577,  
1137 <https://doi.org/10.1029/2019GC008545>, 2019.

1138 Kohn, M. J.: Comment: tooth enamel mineralization in ungulates: implications for recovering a primary  
1139 isotopic time-series, by BH Passey and TE Cerling (2002), *Geochimica et Cosmochimica Acta*, 68(2),  
1140 403–405, 2004.

1141 Lauretano, V., Zachos, J. C. and Lourens, L. J.: Orbitally Paced Carbon and Deep-Sea Temperature  
1142 Changes at the Peak of the Early Eocene Climatic Optimum, *Paleoceanography and Paleoclimatology*,  
1143 33(10), 1050–1065, <https://doi.org/10.1029/2018PA003422>, 2018.

1144 Lear, C. H., Bailey, T. R., Pearson, P. N., Coxall, H. K. and Rosenthal, Y.: Cooling and ice growth across  
1145 the Eocene-Oligocene transition, *Geology*, 36(3), 251–254, 2008.

1146 LeGrande, A. N. and Schmidt, G. A.: Global gridded data set of the oxygen isotopic composition in  
1147 seawater, *Geophysical research letters*, 33(12), 2006.

1148 Lisiecki, L. E. and Raymo, M. E.: A Pliocene-Pleistocene stack of 57 globally distributed benthic  $\delta^{18}\text{O}$   
1149 records, *Paleoceanography*, 20(1), <https://doi.org/10.1029/2004PA001071>, 2005.

1150 *Lourens, L. J., Sluijs, A., Kroon, D., Zachos, J. C., Thomas, E., Röhl, U., Bowles, J. and Raffi, I.:*  
1151 *Astronomical pacing of late Palaeocene to early Eocene global warming events, *Nature*, 435(7045),*  
1152 *1083–1087, <https://doi.org/10.1038/nature03814>, 2005.*

- 1153 Lourens, L. J., Becker, J., Bintanja, R., Hilgen, F. J., Tuenter, E., Van de Wal, R. S. and Ziegler, M.: Linear  
1154 and non-linear response of late Neogene glacial cycles to obliquity forcing and implications for the  
1155 Milankovitch theory, *Quaternary Science Reviews*, 29(1–2), 352–365, 2010.
- 1156 McArthur, J. M., Howarth, R. J. and Shields, G. A.: Strontium isotope stratigraphy, *The geologic time scale*,  
1157 1, 127–144, 2012.
- 1158 Meckler, A. N., Ziegler, M., Millán, M. I., Breitenbach, S. F. and Bernasconi, S. M.: Long-term performance  
1159 of the Kiel carbonate device with a new correction scheme for clumped isotope measurements, *Rapid  
1160 Communications in Mass Spectrometry*, 28(15), 1705–1715, 2014.
- 1161 Merz, B. and Thieken, A. H.: Separating natural and epistemic uncertainty in flood frequency analysis,  
1162 *Journal of Hydrology*, 309(1–4), 114–132, 2005.
- 1163 Meyers, S. R.: Astrochron: An R package for astrochronology, [http://cran.r-](http://cran.r-project.org/package=astrochron)  
1164 [project.org/package=astrochron](http://cran.r-project.org/package=astrochron).  
1165 <http://scholar.google.com/scholar?cluster=14876361610707754388&hl=en&oi=scholar>, last access: 30  
1166 May 2017, 2014.
- 1167 Meyers, S. R.: Cyclostratigraphy and the problem of astrochronologic testing, *Earth-Science Reviews*, 190,  
1168 190–223, <https://doi.org/10.1016/j.earscirev.2018.11.015>, 2019.
- 1169 Miyaji, T., Tanabe, K., Matsushima, Y., Sato, S., Yokoyama, Y. and Matsuzaki, H.: Response of daily and  
1170 annual shell growth patterns of the intertidal bivalve *Phacosoma japonicum* to Holocene coastal climate  
1171 change in Japan, *Palaeogeography, Palaeoclimatology, Palaeoecology*, 286(3), 107–120,  
1172 <https://doi.org/10.1016/j.palaeo.2009.11.032>, 2010.
- 1173 Mook, W. G.: Stable carbon and oxygen isotopes of natural waters in the Netherlands, *Isotope hydrology*,  
1174 1970, 163–190, 1970.
- 1175 Morgan, V. and van Ommen, T. D.: Seasonality in late-Holocene climate from ice-core records, *The  
1176 Holocene*, 7(3), 351–354, <https://doi.org/10.1177/095968369700700312>, 1997.
- 1177 Mosley-Thompson, E., Thompson, L. G., Dai, J., Davis, M. and Lin, P. N.: Climate of the last 500 years:  
1178 High resolution ice core records, *Quaternary Science Reviews*, 12(6), 419–430,  
1179 [https://doi.org/10.1016/S0277-3791\(05\)80006-X](https://doi.org/10.1016/S0277-3791(05)80006-X), 1993.
- 1180 Müller, I. A., Fernandez, A., Radke, J., van Dijk, J., Bowen, D., Schwieters, J. and Bernasconi, S. M.:  
1181 Carbonate clumped isotope analyses with the long-integration dual-inlet (LIDI) workflow: scratching at  
1182 the lower sample weight boundaries: LIDI as key for more precise analyses on much less carbonate  
1183 material, *Rapid Communications in Mass Spectrometry*, 31(12), 1057–1066,  
1184 <https://doi.org/10.1002/rcm.7878>, 2017.
- 1185 Noorbergen, L. J., Abels, H. A., Hilgen, F. J., Robson, B. E., Jong, E. de, Dekkers, M. J., Krijgsman, W.,  
1186 Smit, J., Collinson, M. E. and Kuiper, K. F.: Conceptual models for short-eccentricity-scale climate control  
1187 on peat formation in a lower Palaeocene fluvial system, north-eastern Montana (USA), *Sedimentology*,  
1188 65(3), 775–808, <https://doi.org/10.1111/sed.12405>, 2018.
- 1189 O'Brien, C. L., Robinson, S. A., Pancost, R. D., Sinninghe Damsté, J. S., Schouten, S., Lunt, D. J., Alsenz,  
1190 H., Bornemann, A., Bottini, C., Brassell, S. C., Farnsworth, A., Forster, A., Huber, B. T., Inglis, G. N.,  
1191 Jenkyns, H. C., Linnert, C., Littler, K., Markwick, P., McAnena, A., Mutterlose, J., Naafs, B. D. A.,  
1192 Püttmann, W., Sluijs, A., van Helmond, N. A. G. M., Vellekoop, J., Wagner, T., and Wrobel, N. E.:

- 1193 [Cretaceous sea-surface temperature evolution: Constraints from TEX 86 and planktonic foraminiferal](https://doi.org/10.1016/j.earscirev.2017.07.012)  
 1194 [oxygen isotopes. 172, 224–247, https://doi.org/10.1016/j.earscirev.2017.07.012, 2017.](https://doi.org/10.1016/j.earscirev.2017.07.012)
- 1195 O'Donnell, M. S. and Ignizio, D. A.: Bioclimatic predictors for supporting ecological applications in the  
 1196 conterminous United States, US Geological Survey Data Series, 691(10), 2012.
- 1197 Passey, B. H. and Cerling, T. E.: Tooth enamel mineralization in ungulates: implications for recovering a  
 1198 primary isotopic time-series, *Geochimica et Cosmochimica Acta*, 66(18), 3225–3234, 2002.
- 1199 Petersen, S. V., Tabor, C. R., Lohmann, K. C., Poulsen, C. J., Meyer, K. W., Carpenter, S. J., Erickson, J.  
 1200 M., Matsunaga, K. K., Smith, S. Y. and Sheldon, N. D.: Temperature and salinity of the Late Cretaceous  
 1201 western interior seaway, *Geology*, 44(11), 903–906, 2016.
- 1202 Philander, S. G. H.: El Nino southern oscillation phenomena, *Nature*, 302(5906), 295–301, 1983.
- 1203 R Core Team: R: A language and environment for statistical computing. R Foundation for Statistical  
 1204 Computing, Vienna, Austria. <http://www.R-project.org/>, 2013.
- 1205 Rodríguez-Sanz, L., Bernasconi, S. M., Marino, G., Heslop, D., Müller, I. A., Fernandez, A., Grant, K. M.  
 1206 and Rohling, E. J.: Penultimate deglacial warming across the Mediterranean Sea revealed by clumped  
 1207 isotopes in foraminifera, *Scientific Reports*, 7(1), 1–11, <https://doi.org/10.1038/s41598-017-16528-6>,  
 1208 2017.
- 1209 Rohling, E. J.: Oxygen isotope composition of seawater, *The Encyclopedia of Quaternary Science*.  
 1210 Amsterdam: Elsevier, 2, 915–922, 2013.
- 1211 Sano, Y., Kobayashi, S., Shirai, K., Takahata, N., Matsumoto, K., Watanabe, T., Sowa, K. and Iwai, K.:  
 1212 Past daily light cycle recorded in the strontium/calcium ratios of giant clam shells, *Nature*  
 1213 *Communications*, 3, 761, 2012.
- 1214 Sato, S.: Temporal change of life-history traits in fossil bivalves: an example of *Phacosoma japonicum* from  
 1215 the Pleistocene of Japan, *Palaeogeography, Palaeoclimatology, Palaeoecology*, 154(4), 313–323,  
 1216 [https://doi.org/10.1016/S0031-0182\(99\)00106-6](https://doi.org/10.1016/S0031-0182(99)00106-6), 1999.
- 1217 Schmitt, J., Schneider, R., Elsig, J., Leuenberger, D., Laurantou, A., Chappellaz, J., Kohler, P., Joos, F.,  
 1218 Stocker, T. F., Leuenberger, M. and Fischer, H.: Carbon Isotope Constraints on the Deglacial CO<sub>2</sub> Rise  
 1219 from Ice Cores, *Science*, 336(6082), 711–714, <https://doi.org/10.1126/science.1217161>, 2012.
- 1220 Scholz, D. and Hoffmann, D. L.: StalAge—An algorithm designed for construction of speleothem age models,  
 1221 *Quaternary Geochronology*, 6(3–4), 369–382, 2011.
- 1222 Schöne, B. R.: The curse of physiology—challenges and opportunities in the interpretation of geochemical  
 1223 data from mollusk shells, *Geo-Marine Letters*, 28(5–6), 269–285, 2008.
- 1224 Schöne, B. R., Fiebig, J., Pfeiffer, M., Gleß, R., Hickson, J., Johnson, A. L., Dreyer, W. and Oschmann, W.:  
 1225 Climate records from a bivalved *Methuselah* (*Arctica islandica*, Mollusca; Iceland), *Palaeogeography,*  
 1226 *Palaeoclimatology, Palaeoecology*, 228(1–2), 130–148, 2005.
- 1227 Schöne, B. R., Rodland, D. L., Fiebig, J., Oschmann, W., Goodwin, D., Flessa, K. W. and Dettman, D.:  
 1228 Reliability of multitaxon, multiproxy reconstructions of environmental conditions from accretionary  
 1229 biogenic skeletons, *The Journal of geology*, 114(3), 267–285, 2006.

- 1230 Scourse, J., Richardson, C., Forsythe, G., Harris, I., Heinemeier, J., Fraser, N., Briffa, K. and Jones, P.:  
 1231 First cross-matched floating chronology from the marine fossil record: data from growth lines of the long-  
 1232 lived bivalve mollusc *Arctica islandica*, *The Holocene*, 16(7), 967–974,  
 1233 <https://doi.org/10.1177/0959683606h1987rp>, 2006.
- 1234 Sha, L., Mahata, S., Duan, P., Luz, B., Zhang, P., Baker, J., Zong, B., Ning, Y., Brahim, Y. A., Zhang, H.,  
 1235 Edwards, R. L. and Cheng, H.: A novel application of triple oxygen isotope ratios of speleothems,  
 1236 *Geochimica et Cosmochimica Acta*, 270, 360–378, <https://doi.org/10.1016/j.gca.2019.12.003>, 2020.
- 1237 Shao, D., Mei, Y., Yang, Z., Wang, Y., Yang, W., Gao, Y., Yang, L. and Sun, L.: Holocene ENSO variability  
 1238 in the South China Sea recorded by high-resolution oxygen isotope records from the shells of *Tridacna*  
 1239 spp., *Scientific Reports*, 10(1), 3921, <https://doi.org/10.1038/s41598-020-61013-2>, 2020.
- 1240 Sinnesael, M., De Vleeschouwer, D., Zeeden, C., Batenburg, S. J., Da Silva, A.-C., de Winter, N. J.,  
 1241 Dinarès-Turell, J., Drury, A. J., Gambacorta, G. and Hilgen, F. J.: The Cyclostratigraphy Intercomparison  
 1242 Project (CIP): consistency, merits and pitfalls, *Earth-Science Reviews*, 102965, 2019.
- 1243 Stap, L., Lourens, L. J., Thomas, E., Sluijs, A., Bohaty, S. and Zachos, J. C.: High-resolution deep-sea  
 1244 carbon and oxygen isotope records of Eocene Thermal Maximum 2 and H2, *Geology*, 38(7), 607–610,  
 1245 2010.
- 1246 Steffensen, J. P., Andersen, K. K., Bigler, M., Clausen, H. B., Dahl-Jensen, D., Fischer, H., Goto-Azuma,  
 1247 K., Hansson, M., Johnsen, S. J. and Jouzel, J.: High-resolution Greenland ice core data show abrupt  
 1248 climate change happens in few years, *Science*, 321(5889), 680–684, 2008.
- 1249 Steuber, T., Rauch, M., Masse, J.-P., Graaf, J. and Malkoč, M.: Low-latitude seasonality of Cretaceous  
 1250 temperatures in warm and cold episodes, *Nature*, 437(7063), 1341–1344,  
 1251 <https://doi.org/10.1038/nature04096>, 2005.
- 1252 Surge, D., Lohmann, K. C. and Dettman, D. L.: Controls on isotopic chemistry of the American oyster,  
 1253 *Crassostrea virginica*: implications for growth patterns, *Palaeogeography, Palaeoclimatology,*  
 1254 *Palaeoecology*, 172(3), 283–296, 2001.
- 1255 [Tagliavento, M., John, C. M., and Stemmerik, L.: Tropical temperature in the Maastrichtian Danish Basin:  
 1256 Data from coccolith  \$\Delta 47\$  and  \$\delta 18O\$ , 47, 1074–1078, 2019.](#)
- 1257 Titschack, J., Zuschin, M., Spötl, C. and Baal, C.: The giant oyster *Hytotissa hyotis* from the northern Red  
 1258 Sea as a decadal-scale archive for seasonal environmental fluctuations in coral reef habitats, *Coral*  
 1259 *Reefs*, 29(4), 1061–1075, 2010.
- 1260 Treble, P., Shelley, J. M. G. and Chappell, J.: Comparison of high resolution sub-annual records of trace  
 1261 elements in a modern (1911–1992) speleothem with instrumental climate data from southwest Australia,  
 1262 *Earth and Planetary Science Letters*, 216(1), 141–153, [https://doi.org/10.1016/S0012-821X\(03\)00504-1](https://doi.org/10.1016/S0012-821X(03)00504-1),  
 1263 2003.
- 1264 Tsukakoshi, Y.: Sampling variability and uncertainty in total diet studies, *Analyst*, 136(3), 533–539,  
 1265 <https://doi.org/10.1039/C0AN00397B>, 2011.
- 1266 Tudhope, A. W.: Variability in the El Niño-Southern Oscillation Through a Glacial-Interglacial Cycle,  
 1267 *Science*, 291(5508), 1511–1517, <https://doi.org/10.1126/science.1057969>, 2001.



- 1268 Ullmann, C. V., Wiechert, U. and Korte, C.: Oxygen isotope fluctuations in a modern North Sea oyster  
1269 (*Crassostrea gigas*) compared with annual variations in seawater temperature: Implications for  
1270 palaeoclimate studies, *Chemical Geology*, 277(1), 160–166, 2010.
- 1271 [van Dam, J. A. and Reichart, G. J.: Oxygen and carbon isotope signatures in late Neogene horse teeth](#)  
1272 [from Spain and application as temperature and seasonality proxies, \*Palaeogeography,\*](#)  
1273 [Palaeoclimatology, Palaeoecology](#), 274(1–2), 64–81, [https://doi.org/10.1016/j.palaeo.2008.12.022.](https://doi.org/10.1016/j.palaeo.2008.12.022.2009)  
1274 [2009.](#)
- 1275 Van Rampelbergh, M., Verheyden, S., Allan, M., Quinif, Y., Keppens, E. and Claeys, P.: Seasonal variations  
1276 recorded in cave monitoring results and a 10 year monthly resolved speleothem  $\delta^{18}\text{O}$  and  $\delta^{13}\text{C}$  record  
1277 from the Han-sur-Lesse cave, Belgium, *Climate of the Past Discussions*, 10, 1821–1856, 2014.
- 1278 Vansteenberghe, S., Verheyden, S., Cheng, H., Edwards, R. L., Keppens, E. and Claeys, P.: Paleoclimate  
1279 in continental northwestern Europe during the Eemian and early Weichselian (125–97 ka): insights from  
1280 a Belgian speleothem, *Clim. Past*, 12(7), 1445–1458, <https://doi.org/10.5194/cp-12-1445-2016>, 2016.
- 1281 Vansteenberghe, S., Winter, N. de, Sinnesael, M., Verheyden, S., Goderis, S., Malderen, S. J. M. V.,  
1282 Vanhaecke, F. and Claeys, P.: Reconstructing seasonality through stable isotope and trace element  
1283 analysis of the Proserpine stalagmite, Han-sur-Lesse Cave, Belgium: indications for climate-driven  
1284 changes during the last 400 years, *Climate of the Past Discussions*, 1–32, [https://doi.org/10.5194/cp-](https://doi.org/10.5194/cp-2019-78)  
1285 [2019-78](#), 2019.
- 1286 Veizer, J. and Prokoph, A.: Temperatures and oxygen isotopic composition of Phanerozoic oceans, *Earth-*  
1287 *Science Reviews*, 146, 92–104, <https://doi.org/10.1016/j.earscirev.2015.03.008>, 2015.
- 1288 Vleeschouwer, D. D., Vahlenkamp, M., Crucifix, M. and Pälike, H.: Alternating Southern and Northern  
1289 Hemisphere climate response to astronomical forcing during the past 35 m.y., *Geology*, 45(4), 375–378,  
1290 <https://doi.org/10.1130/G38663.1>, 2017.
- 1291 Warter, V. and Müller, W.: Daily growth and tidal rhythms in Miocene and modern giant clams revealed via  
1292 ultra-high resolution LA-ICPMS analysis—A novel methodological approach towards improved  
1293 sclerochemistry, *Palaeogeography, Palaeoclimatology, Palaeoecology*, 465, 362–375, 2017.
- 1294 Westerhold, T., Marwan, N., Drury, A. J., Liebrand, D., Agnini, C., Anagnostou, E., Barnet, J. S., Bohaty,  
1295 S. M., De Vleeschouwer, D. and Florindo, F.: An astronomically dated record of Earth's climate and its  
1296 predictability over the last 66 million years, *Science*, 369(6509), 1383–1387, 2020.
- 1297 Wilkinson, B. H. and Ivany, L. C.: Paleoclimatic inference from stable isotope profiles of accretionary  
1298 biogenic hardparts – a quantitative approach to the evaluation of incomplete data, *Palaeogeography,*  
1299 *Palaeoclimatology, Palaeoecology*, 185(1), 95–114, [https://doi.org/10.1016/S0031-0182\(02\)00279-1](https://doi.org/10.1016/S0031-0182(02)00279-1),  
1300 2002.
- 1301 [Williams, M., Haywood, A. M., Harper, E. M., Johnson, A. L. A., Knowles, T., Leng, M. J., Lunt, D. J.,](#)  
1302 [Okamura, B., Taylor, P. D., and Zalasiewicz, J.: Pliocene climate and seasonality in North Atlantic shelf](#)  
1303 [seas, \*Philosophical Transactions of the Royal Society A: Mathematical, Physical and Engineering\*](#)  
1304 [Sciences](#), 367, 85–108, <https://doi.org/10.1098/rsta.2008.0224>, 2009.
- 1305 Yan, H., Liu, C., An, Z., Yang, W., Yang, Y., Huang, P., Qiu, S., Zhou, P., Zhao, N. and Fei, H.: Extreme  
1306 weather events recorded by daily to hourly resolution biogeochemical proxies of marine giant clam shells,  
1307 *Proceedings of the National Academy of Sciences*, 2020.

1308 [Zhang, L., Tang Wilson H., Zhang Lulu, and Zheng Jianquo: Reducing Uncertainty of Prediction from](#)  
1309 [Empirical Correlations, \*Journal of Geotechnical and Geoenvironmental Engineering\*, 130, 526–534.](#)  
1310 [https://doi.org/10.1061/\(ASCE\)1090-0241\(2004\)130:5\(526\)](https://doi.org/10.1061/(ASCE)1090-0241(2004)130:5(526)), 2004.